CELL BIOLOGY

The *parkin-coregulated gene* product PACRG promotes TNF signaling by stabilizing LUBAC

Jens Meschede[1], Maria Šadić[2]*, Nikolas Furthmann[1]*, Tim Miedema[1]*, Dominik A. Sehr[1], A. Kathrin Müller-Rischart[2†], Verian Bader[1], Lena A. Berlemann[1], Anna Pilsl[2‡], Anita Schlierf[2§], Katalin Barkovits[3], Barbara Kachholz[1], Katrin Rittinger[4], Fumiyo Ikeda[5], Katrin Marcus[3], Liliana Schaefer[6], Jörg Tatzelt[2,7], Konstanze F. Winklhofer[1,2]||

The *Parkin-coregulated gene* (*PACRG*), which encodes a protein of unknown function, shares a bidirectional promoter with *Parkin* (*PRKN*), which encodes an E3 ubiquitin ligase. Because PRKN is important in mitochondrial quality control and protection against stress, we tested whether PACRG also affected these pathways in various cultured human cell lines and in mouse embryonic fibroblasts. PACRG did not play a role in mitophagy but did play a role in tumor necrosis factor (TNF) signaling. Similarly to Parkin, PACRG promoted nuclear factor κB (NF-κB) activation in response to TNF. TNF-induced nuclear translocation of the NF-κB subunit p65 and NF-κB–dependent transcription were decreased in PACRG-deficient cells. Defective canonical NF-κB activation in the absence of PACRG was accompanied by a decrease in linear ubiquitylation mediated by the linear ubiquitin chain assembly complex (LUBAC), which is composed of the two E3 ubiquitin ligases HOIP and HOIL-1L and the adaptor protein SHARPIN. Upon TNF stimulation, PACRG was recruited to the activated TNF receptor complex and interacted with LUBAC components. PACRG functionally replaced SHARPIN in this context. In SHARPIN-deficient cells, PACRG prevented LUBAC destabilization, restored HOIP-dependent linear ubiquitylation, and protected cells from TNF-induced apoptosis. This function of PACRG in positively regulating TNF signaling may help to explain the association of *PACRG* and *PRKN* polymorphisms with an increased susceptibility to intracellular pathogens.

INTRODUCTION

The gene that encodes Parkin, a RING-between-RING (RBR) E3 ubiquitin ligase associated with autosomal recessive parkinsonism, is linked in a head-to-head arrangement to another gene on the opposite DNA strand with which it shares a 5′ core bidirectional promoter (Fig. 1A) (*1*). This gene has been named *Parkin-coregulated gene* (*PACRG*). Parkin can prevent cell death in various stress paradigms, and several mechanisms seem to contribute to its beneficial effects on cell viability. Parkin induces the removal of depolarized mitochondria in a pathway that depends on the mitochondrial serine-threonine kinase PINK1 [phosphatase and tensin homolog (PTEN)–induced kinase 1], which is required to recruit and activate Parkin [reviewed in (*2*–*5*)]. Parkin also promotes the degradation of specific substrates to prevent unfavorable effects upon their accumulation [reviewed in (*6*)]. Moreover, Parkin attenuates cell death pathways by nondegradative ubiquitylation [reviewed in (*7*, *8*)]. The function of PACRG and a possible role in pathways regulated by Parkin remains poorly understood. PACRG has been allocated to the Armadillo-like helical domain–containing family of proteins but lacks domains that indicate its function. PACRG is highly conserved and so far has mainly been linked to the functions of motile and nonmotile (primary) cilia (*9*–*14*). PACRG has also been analyzed in the context of Parkinson's disease (PD). There is no evidence for a genetic link between mutations in *PACRG* and familial PD; however, PACRG is a component of Lewy bodies in brain sections from patients with sporadic PD or dementia with Lewy bodies (*15*, *16*). Similarly to Parkin, PACRG suppresses cell death induced by the overexpression of Pael-R, a G protein–coupled receptor that is a Parkin substrate (*15*, *17*). Moreover, polymorphisms in the regulatory region shared by *PRKN* and *PACRG* are a common risk factor for infection with intracellular bacteria, such as *Mycobacterium tuberculosis* or *Salmonella enterica* serovars Typhi and Paratyphi (*18*–*21*), suggesting a role for Parkin and PACRG in immune signaling.

We previously found that the prosurvival function of Parkin depends on nuclear factor κB (NF-κB) essential modulator (NEMO), a key positive regulator of the NF-κB signaling pathway (*22*). Parkin increases the linear ubiquitylation of NEMO by the linear ubiquitin chain assembly complex (LUBAC), which is composed of the two RBR E3 ubiquitin ligases HOIP and HOIL-1L and the adaptor protein SHARPIN [SH3 and multiple ankyrin repeat domains (SHANK)–associated RH domain interactor]. The absence of either NEMO or HOIP, the catalytic component of LUBAC, prevents Parkin from blocking stress-induced cell death (*22*). Supporting a role of Parkin in this pathway, tumor necrosis factor (TNF)–induced activation of NF-κB is decreased in Parkin-deficient cells (*22*).

On the basis of the fact that bidirectional promoters are known to drive the expression of genes that cooperate in common pathways or share biological functions (*23*), we asked whether PACRG played a role in pathways associated with the function of Parkin. Our study revealed that PACRG promoted canonical NF-κB signaling

[1]Molecular Cell Biology, Institute of Biochemistry and Pathobiochemistry, Ruhr University Bochum, 44801 Bochum, Germany. [2]Neurobiochemistry, Adolf Butenandt Institute, Ludwig Maximilians University, 80336 Munich, Germany. [3]Medizinisches Proteom-Center, Ruhr University Bochum, 44801 Bochum, Germany. [4]The Francis Crick Institute, 1 Midland Road, London NW1 1AT, UK. [5]Institute of Molecular Biotechnology (IMBA), 1030 Vienna, Austria. [6]Pharmacenter Frankfurt/ZAFES, Institute for General Pharmacology and Toxicology, Goethe University, 60590 Frankfurt am Main, Germany. [7]Biochemistry of Neurodegenerative Diseases, Institute of Biochemistry and Pathobiochemistry, Ruhr University Bochum, 44801 Bochum, Germany.
*These authors contributed equally to this work.
†Present address: Center for Integrated Protein Science, Department of Biology II, Ludwig Maximilians University, Martinsried, Germany.
‡Present address: Thermo Fisher Scientific GENEART GmbH, Regensburg, Germany.
§Present address: Novartis Institutes for Biomedical Research, Novartis Pharma AG, Basel, Switzerland.
||Corresponding author. Email: konstanze.winklhofer@rub.de

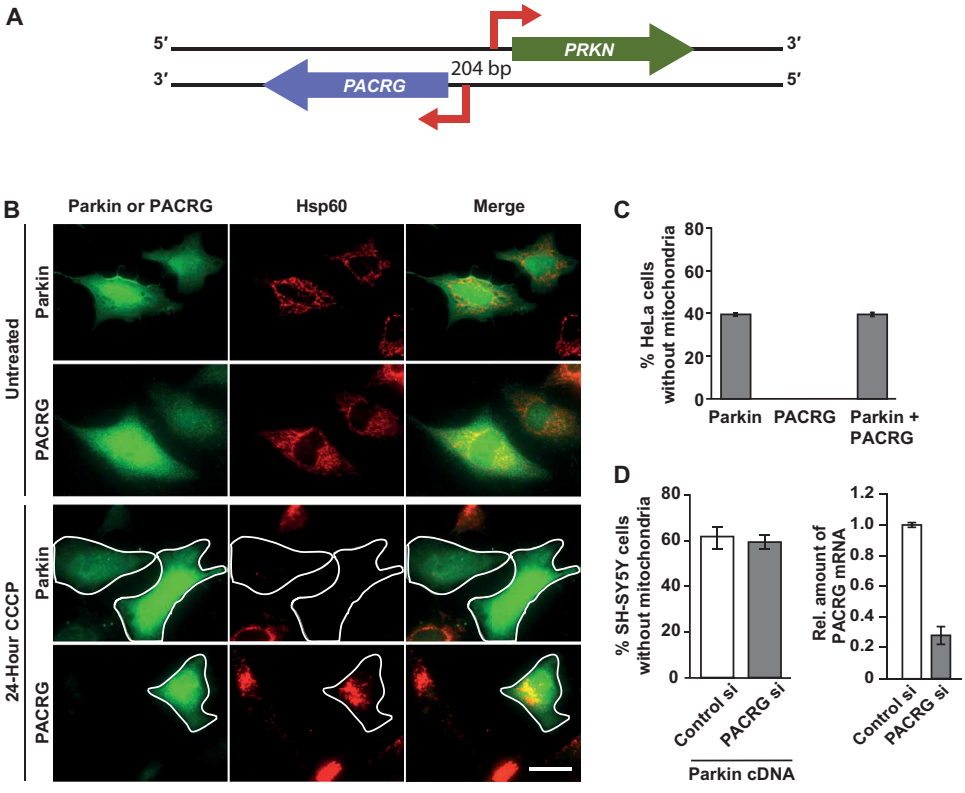

Fig. 1. PACRG does not influence mitophagy. (**A**) Schematic representation of the *PRKN* and *PACRG* locus. The genes encoding Parkin and PACRG are linked in a head-to-head arrangement on opposite DNA strands and share a 5′ core bidirectional promoter of 204 base pairs. (**B**) Representative immunofluorescence images of HeLa cells transiently expressing HA-tagged PACRG or Parkin and treated with CCCP to induce mitochondrial depolarization and subsequent degradation. Fixed cells were analyzed by indirect immunofluorescence using either the Parkin-specific antibody PRK8 or an HA antibody to detect PACRG and an Hsp60-specific antibody to visualize mitochondria. Scale bar, 100 μm. (**C**) Quantification of CCCP-induced mitochondrial clearance in HeLa cells expressing Parkin, PACRG, or both Parkin and PACRG. (**D**) Quantification of CCCP-induced mitochondrial clearance in SH-SY5Y cells transfected with control or PACRG siRNAs together with Parkin cDNA. PACRG knockdown efficiency was determined by real-time reverse transcription (RT)–PCR using exon-flanking PACRG-specific primers. Data represent the means ± SEM of at least three independent experiments, each performed in triplicate. At least 300 transfected cells were counted per condition. For statistical analysis Mann-Whitney *U* test was performed.

induced by TNF through an interaction with LUBAC. PACRG could functionally replace the adaptor protein SHARPIN in cellular models, suggesting a role of PACRG in stabilizing LUBAC as a scaffold protein. Because TNF plays a crucial role in the protection against *Mycobacterium* and *Salmonella* infections (*24*–*26*), our findings provide a rationale for the association of mutations in *PRKN* and *PACRG* with an increased risk for intracellular bacterial infections.

RESULTS

PACRG does not influence mitophagy

Parkin promotes the clearance of depolarized mitochondria in a pathway that depends on the mitochondrial kinase PINK1, which is imported into healthy mitochondria (*27*, *28*). Accumulation of PINK1 on the outer membrane of damaged mitochondria results in the phosphorylation of ubiquitin that is basally linked to proteins at the mitochondrial outer membrane, leading to the recruitment and activation of Parkin and Parkin-mediated ubiquitylation of several mitochondrial outer membrane proteins. As a consequence, autophagy adaptors are recruited to eliminate damaged mitochondria by selective autophagy [reviewed in (*2*–*5*)]. First, we tested whether PACRG played a role in PINK1- and Parkin-induced mitophagy. For this analysis, we used HeLa cells, which produce endogenous PINK1 but not Parkin or PACRG (*29*). We treated HeLa cells transiently expressing Parkin or PACRG, or both, with CCCP (carbonyl cyanide 3-chlorophenylhydrazone) to induce mitochondrial depolarization. CCCP treatment induced mitochondrial clearance in cells expressing only Parkin but not in cells expressing only PACRG (Fig. 1, B and C). Coexpression of PACRG with Parkin did not increase or decrease mitophagy in response to CCCP treatment compared with cells expressing Parkin alone (Fig. 1C). We also tested for a possible effect of endogenous PACRG on PINK1- and Parkin-induced mitophagy in SH-SY5Y cells that were transiently expressing Parkin and that had been transfected with a mix of small interfering RNAs (siRNA) targeting PACRG. We observed no difference in the efficiency of CCCP-induced mitochondrial clearance between control and PACRG knockdown cells (Fig. 1D). In conclusion, PACRG seemed not to play a relevant role in PINK1- and Parkin-induced mitophagy because neither PACRG overexpression nor PACRG silencing influenced mitophagy in response to mitochondrial depolarization.

PACRG promotes canonical NF-κB signaling

Parkin has been shown to promote NF-κB signaling in response to various stimuli (*22*, *30*–*33*). To test whether PACRG had an impact on this pathway, we performed NF-κB luciferase reporter assays. Similarly to Parkin, PACRG induced a fivefold increase in luciferase activity both in unstimulated and TNF-treated human embryonic kidney (HEK) 293T cells (Fig. 2A). PACRG also induced NF-κB–dependent transcription in mouse embryonic fibroblasts (MEFs) from Parkin knockout (KO) mice, indicating that the effect of PACRG on NF-κB activation did not depend on Parkin (Fig. 2B).

Binding of TNF to its receptor, TNFR1, at the plasma membrane stimulates NF-κB signaling by activating the inhibitor of NF-κB (IκB) kinase (IKK) complex, comprising the regulatory component NEMO and the kinases IKKα and IKKβ. IKKs phosphorylate the NF-κB inhibitor IκBα, which is subsequently ubiquitylated and degraded by the proteasome. NF-κB heterodimers are thereby released from their inhibitory binding and can translocate to the nucleus to promote or repress the transcription of target genes. Nuclear translocation of the NF-κB subunit p65 (also known as RelA) in response to TNF treatment was quantified by immunocytochemistry in PACRG-silenced SH-SY5Y cells in comparison to

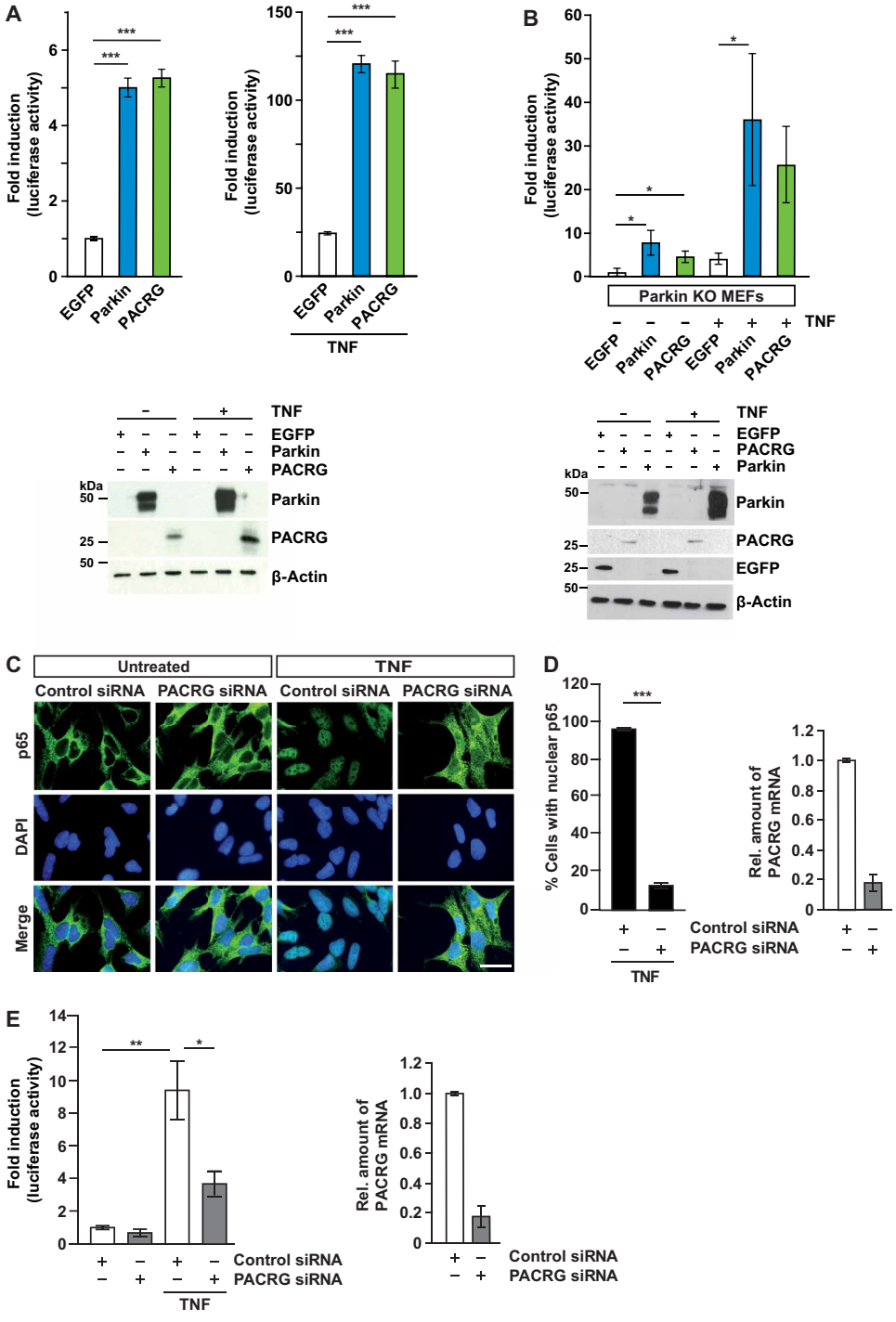

Fig. 2. PACRG deficiency impairs TNF-induced NF-κB activation. (**A**) HEK293T cells were transfected with PACRG, Parkin, or EGFP (negative control) and an NF-κB luciferase reporter construct. Luciferase activity was quantified in lysates of untreated and TNF-treated cells, with luciferase activity in untreated EGFP-expressing cells set to 1. Quantifications were based on at least three independent experiments, each performed in triplicate. Expression of proteins from the transfected plasmids was verified by Western blotting for Parkin and PACRG. β-Actin is a loading control. Data represent the means ± SEM of 7 to 12 independent experiments. For statistical analysis, ANOVA followed by Tukey's multiple comparison test was performed. (**B**) Parkin KO MEFs were transfected with either PACRG or Parkin and an NF-κB luciferase reporter construct. Luciferase activity was measured in lysates of untreated and TNF-treated cells as in (A). Data represent the means ± SEM of four to five independent experiments. For statistical analysis, one-tailed Mann-Whitney *U* test was performed. (**C**) Representative immunofluorescence images showing p65 localization in SH-SY5Y cells transfected with control or PACRG-specific siRNAs and treated with TNF. Nuclei were labeled with DAPI. Scale bar, 100 μm. (**D**) Quantification of TNF-induced nuclear translocation of p65 in control and PACRG knockdown SH-SY5Y cells based on three independent experiments, each performed in duplicate. PACRG knockdown efficiency was determined using real-time RT-PCR. Data represent the means ± SEM of three to five independent experiments. For statistical analysis, one-tailed Mann-Whitney *U* test was performed. (**E**) HEK293T cells were transfected with either control or PACRG-specific siRNAs and an NF-κB luciferase reporter construct and then treated with TNF or left untreated. Luciferase activity in cell lysates was measured. Data represent the means ± SEM of three independent experiments, each performed in duplicate. For statistical analysis, one-tailed Mann-Whitney *U* test was performed. PACRG knockdown efficiency was determined using real-time RT-PCR. $^{*}P \leq 0.05$; $^{**}P \leq 0.01$; $^{***}P \leq 0.001$.

cells transfected with control siRNA (Fig. 2C). We observed complete translocation of p65 in TNF-treated cells in more than 90% of control cells, but only in 15% of PACRG knockdown cells (Fig. 2D). We verified PACRG knockdown efficiencies by real-time quantitative polymerase chain reaction (PCR) (Fig. 2, D and E, right panels) because we were not able to detect endogenous PACRG with the available antibodies. A similar decrease in TNF-induced nuclear translocation of p65 was observed previously in cells silenced for Parkin expression (*22*). Supporting a role of endogenous PACRG in NF-κB signaling, TNF-induced NF-κB transcriptional activity, as measured by the activity of a luciferase reporter, was significantly decreased in PACRG knockdown cells (Fig. 2E). The luciferase reporter assays were performed 16 hours after TNF treatment, supporting the notion that decreased PACRG abundance decreased rather than only delayed NF-κB activation.

PACRG increases LUBAC-mediated linear ubiquitylation

To gain insight into the mechanism underlying the NF-κB–activating effect of PACRG, we analyzed events upstream of p65 translocation. In PACRG knockdown cells, degradation of IκBα in response to TNF treatment was delayed (Fig. 3A). In a next step, we tested

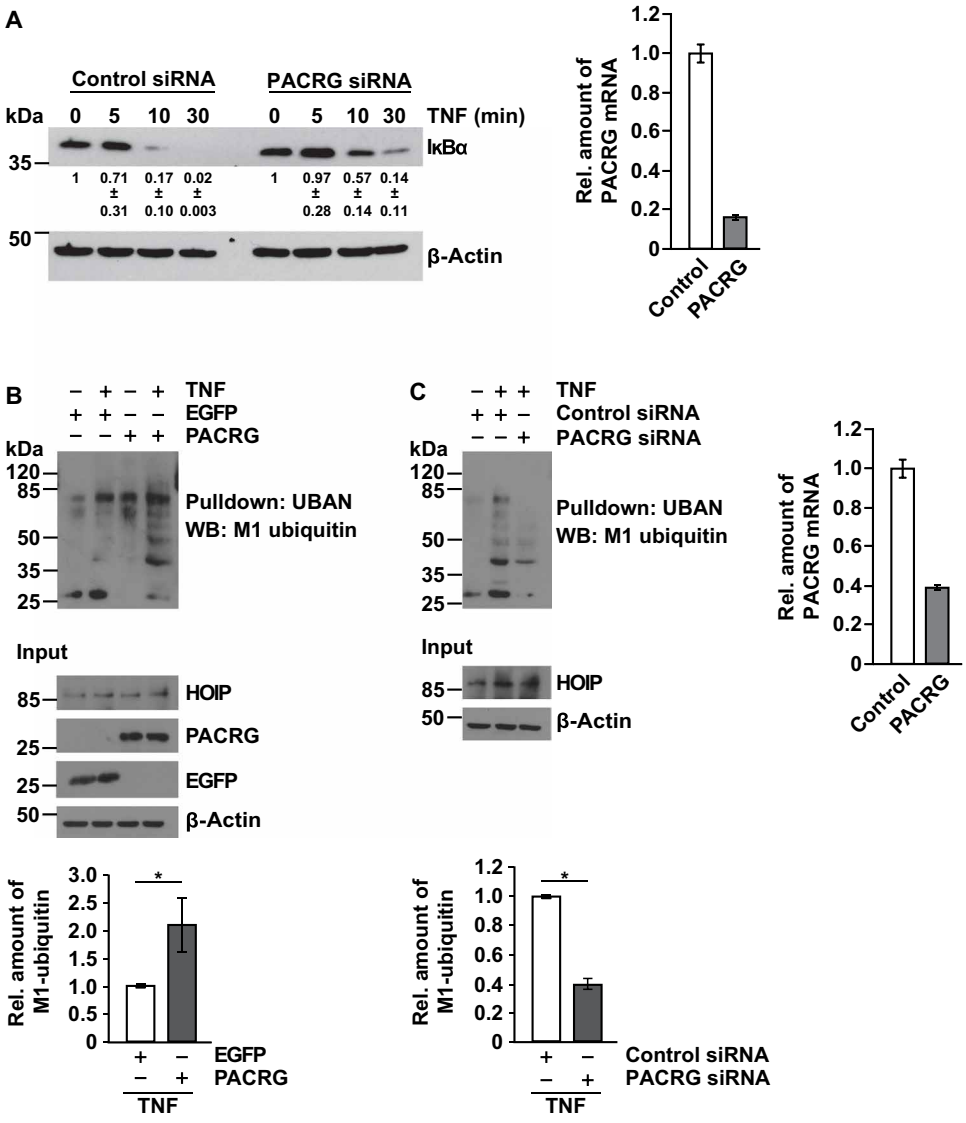

Fig. 3. PACRG increases TNF-induced linear ubiquitylation. (**A**) HEK293T cells transfected with control or PACRG-specific siRNA were treated with TNF 1 day after transfection for the indicated times. Degradation of IκBα was determined by Western blotting (WB) for IκBα. Numbers below the IκBα-reactive bands indicate the mean value of three independent experiments normalized to β-actin levels ± SEM. Graph shows PACRG knockdown efficiency as determined by real-time RT-PCR. (**B**) HEK293T cells were transiently transfected with plasmids encoding the indicated proteins. One day after transfection, cells were treated with TNF and lysed. Lysates generated under denaturing conditions were subjected to pulldown with the Strep-tagged UBAN domain of NEMO, and proteins affinity purified by Strep-Tactin beads were analyzed by immunoblotting with an antibody specific for M1-linked ubiquitin. The input was immunoblotted for HOIP, PACRG, EGFP, and β-actin. Signal intensities of three independent experiments were quantified and normalized to the amount of linear ubiquitin chains in samples with EGFP overexpression and TNF treatment. Data represent the means ± SEM of three independent experiments. For statistical analysis one-tailed Mann-Whitney *U* test was performed. (**C**) HEK293T cells were transiently transfected with the indicated siRNAs. TNF treatment, lysis, and pulldown were performed as in (B). Signal intensities of three independent experiments were quantified and normalized to the amount of linear ubiquitin chains in samples treated with control siRNA and TNF. PACRG knockdown efficiency was determined by real-time RT-PCR. Data represent the means ± SEM of three independent experiments. For statistical analysis, one-tailed Mann-Whitney *U* test was performed. *$P \leq 0.05$

whether PACRG had an impact on TNF-induced linear ubiquitylation mediated by the LUBAC that is required for NF-κB activation after TNFR1 engagement (*34*, *35*). LUBAC is composed of three core subunits, the two RBR E3 ubiquitin ligases HOIP and HOIL-1L and the cofactor SHARPIN [reviewed in (*36*, *37*)]. The catalytic subunit HOIP is the only known E3 ubiquitin ligase capable of assembling ubiquitin chains by covalent linkage of the C-terminal glycine residue of the donor ubiquitin to the N-terminal methionine residue of the acceptor ubiquitin, called linear or M1-linked ubiquitylation. Several LUBAC substrates have been identified, including NEMO, RIPK1 (receptor-interacting protein kinase 1), TRADD, and TNFR1 (*34*, *35*, *38*–*40*). However, there is increasing evidence that LUBAC conjugates M1-linked ubiquitin to pre-existing ubiquitin chains of other linkages, preferably Lys^{63} (K63)–linked polyubiquitin, resulting in hybrid chains (*41*–*43*). Linear ubiquitin chains promote NF-κB activation by acting as a platform for efficient activation of the IKK complex based on the fact that NEMO is not only modified by linear ubiquitylation but also highly specifically binds to M1-linked ubiquitin chains by its UBAN (ubiquitin binding in ABIN and NEMO) domain (*44*). For linear ubiquitylation assays, we used the recombinant UBAN domain of NEMO to specifically pull down linear polyubiquitin chains (*44*–*46*). HEK293T cells overexpressing PACRG (Fig. 3B) or silenced for PACRG expression (Fig. 3C) were lysed under denaturing conditions and then incubated with the recombinant UBAN domain harboring an N-terminal Strep-Tag II, which allowed affinity purification by Strep-Tactin resins (*22*). Proteins purified by this approach were analyzed by immunoblotting using an antibody that specifically detects linear polyubiquitin (*47*). We observed that the extent of linear ubiquitination in TNF-treated cells correlated with the abundance of PACRG. Signal intensities for linear polyubiquitin were decreased in PACRG-silenced cells and increased in PACRG-overexpressing cells (Fig. 3, B and C). In PACRG knockdown cells, the abundance of linear ubiquitin chains in response to TNF was decreased by 60% (Fig. 3C).

HOIP is the catalytically active component of LUBAC and is released from its autoinhibited state by interacting with HOIL-1L and SHARPIN (*38*, *48*, *49*). Coimmunoprecipitation experiments revealed that TNF treatment increased the interaction between PACRG and endogenous HOIP in HEK293T cells (Fig. 4A). After TNF treatment for 180 min, we observed PACRG-reactive higher–molecular weight species, suggesting

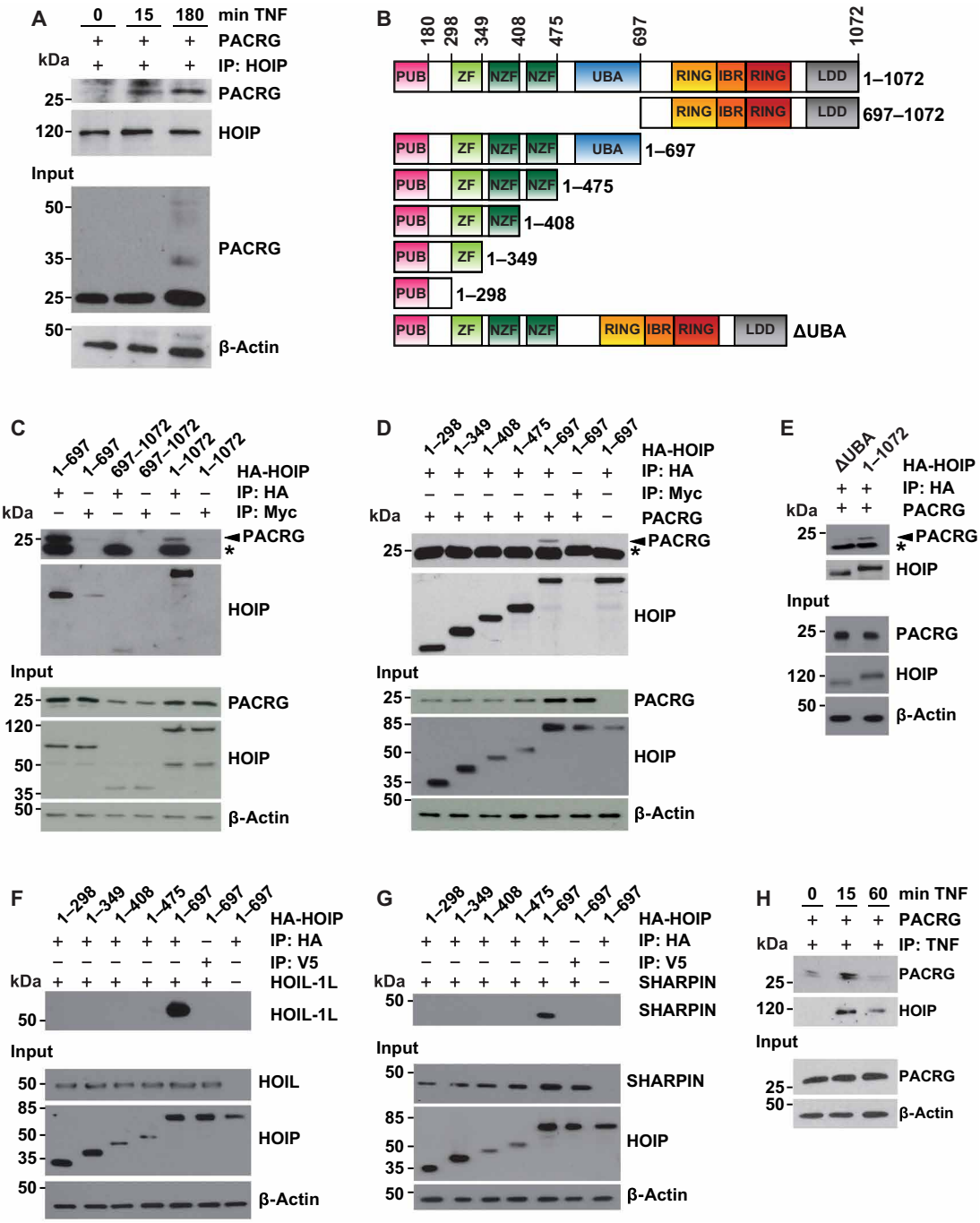

Fig. 4. PACRG binds to LUBAC. (**A**) HEK293T cells were transfected with PACRG and then treated with TNF for the indicated times. Cells were lysed under native conditions, and endogenous HOIP was immunoprecipitated (IP). Immunoprecipitated proteins were detected by Western blotting for PACRG and HOIP. The input was immunoblotted for PACRG and β-actin. (**B**) Schematic presentation of the HOIP constructs used for immunoprecipitation. All constructs included an N-terminal HA tag. PUB, peptide *N*-glycosidase/ubiquitin–associated domain; ZF, zinc finger domain; NZF, nuclear protein localization 4-type zinc finger domain; UBA, ubiquitin-associated domain; RING, really interesting new gene; IBR, in-between RING domain; LDD, linear ubiquitin chain–determining domain. (**C**) HEK293T cells were transfected with either N-terminal (amino acids 1 to 697), C-terminal (amino acids 697 to 1072), or full-length (amino acids 1 to 1072) HA-HOIP together with PACRG. After cell lysis, HOIP was immunoprecipitated and affinity purified. Copurified PACRG was detected by Western blotting using an antibody recognizing PACRG. c-Myc is a negative control. Asterisk notes a nonspecific immunoreactive band. The HOIP IP control and the HOIP input were probed with an antibody specific for HA. (**D**) HEK293T cells were transfected with PACRG and the indicated HOIP constructs. Coimmunoprecipitation experiments were performed as in (C). (**E**) HEK293T cells were transfected with either ΔUBA or full-length HA-HOIP (amino acids 1 to 1072) and PACRG. Coimmunoprecipitation experiments were performed as in (C). (**F** and **G**) HEK293T cells were transfected with the indicated HOIP constructs and either HOIL-1L (F) or SHARPIN (G). Coimmunoprecipitation experiments were performed as in (C). HOIP input levels were detected with an antibody specific for HA. HOIL-1L, SHARPIN, and β-actin were detected with antibodies against the respective proteins. (**H**) HEK293T cells were transfected with PACRG and then treated with FLAG-TNF for the indicated times. After cell lysis, FLAG-TNF was immunoprecipitated and affinity purified. Copurified PACRG and HA-HOIP were detected by Western blotting for PACRG and HA, respectively. All blots are representative of at least three independent experiments.

ubiquitylation of PACRG (Fig. 4A, input). To characterize this direct or indirect interaction between PACRG and HOIP in more detail, we made use of N-terminally hemagglutinin (HA)–tagged HOIP constructs, comprising the N-terminal (amino acids 1 to 697) or C-terminal (amino acids 697 to 1072) half of the protein (Fig. 4B). We expressed full-length, N-terminal, or C-terminal HOIP constructs in HEK293T cells together with PACRG and subjected cellular lysates to immunoprecipitation using HA-binding agarose beads or Myc-binding agarose beads as a control. PACRG coimmunoprecipitated with both full-length HOIP and N-terminal HOIP but not

with C-terminal HOIP (Fig. 4C). Notably, Western blotting of cellular lysates indicated that PACRG abundance was increased in the presence of either full-length or N-terminal HOIP, suggesting stabilization of PACRG by complex formation (Fig. 4, C and D, input), a phenomenon that has been described previously for the LUBAC component SHARPIN (*38*, *48*, *49*).

We then successively removed domains from the C terminus of the N-terminal HOIP construct (Fig. 4B) to more precisely define the region of HOIP that interacted with PACRG. PACRG coimmunoprecipitated with the 1-to-697 HOIP construct, which included the ubiquitin-associated domain (UBA) domain, but not with any of the shorter N-terminal constructs lacking the UBA domain (Fig. 4D). The crucial role of the UBA domain in mediating the interaction with PACRG was confirmed by using an HOIP construct that lacks the UBA domain (Fig. 4E). As a control, coimmunoprecipitation experiments were also performed with HOIP and HOIL-1L or SHARPIN, confirming that these proteins bind to the UBA domain of HOIP in a cellular context (Fig. 4, F and G), consistent with recent in vitro studies using recombinant proteins (*50*, *51*). Supporting binding of PACRG to LUBAC, size exclusion chromatography of cellular lysates revealed that a fraction of PACRG coeluted with the endogenous LUBAC components HOIP, HOIL-1L, and SHARPIN (fig. S1). Moreover, immunoprecipitation experiments using recombinant FLAG-tagged TNF showed that PACRG was recruited to the active TNFR1 complex, similarly to HOIP (Fig. 4H). In conclusion, PACRG directly or indirectly bound to LUBAC, and the UBA domain of HOIP was required for this interaction.

PACRG can compensate for SHARPIN deficiency in cellular models

Binding of the UBL domain of HOIL-1L or SHARPIN to the UBA domain of HOIP releases HOIP from autoinhibition, thereby activating it (*50*–*54*). Like SHARPIN, PACRG has no known catalytic activity and, thus, may function as a scaffold protein. Consequently, we tested whether PACRG could compensate for SHARPIN deficiency. First, we compared the effects of endogenous SHARPIN and PACRG on TNF-induced linear ubiquitylation. HEK293T cells silenced for either SHARPIN or PACRG expression by RNA interference were treated with TNF for 15 min and then lysed under denaturing conditions. Linear ubiquitin chains were affinity purified by UBAN pulldown and subjected to immunoblotting using an antibody specific for M1-linked ubiquitin. Decreasing SHARPIN or PACRG abundance reduced linear ubiquitylation in response to TNF treatment (Fig. 5A). The increased expression of PACRG restored linear ubiquitylation in SHARPIN knockdown cells and vice versa, suggesting that SHARPIN and PACRG had similar effects on TNF-induced linear ubiquitylation (Fig. 5A). Moreover, both PACRG and SHARPIN markedly increased linear ubiquitylation of NEMO, a key substrate of LUBAC (Fig. 5B). As an additional readout, we tested nuclear translocation of p65 in TNF-treated, SHARPIN-silenced cells. PACRG restored defective p65 translocation in SHARPIN-deficient SH-SY5Y cells, and its rescue activity was comparable to that of SHARPIN (fig. S2, A and B). To rule out the possibility that residual SHARPIN expression in siRNA-treated cells contributed to the rescue by PACRG, we used MEFs from SHARPIN KO mice with a spontaneous nonsense mutation in the SHARPIN gene [chronic proliferative dermatitis mutation (cpdm)] (*55*). PACRG fully restored TNF-induced nuclear translocation of p65 in cpdm MEFs (Fig. 5C).

It has been reported previously that SHARPIN deficiency interferes with TNFR1-mediated prosurvival signaling and sensitizes cells to TNF-induced apoptotic cell death (*38*, *48*, *56*, *57*). To address the functional relevance of our observations, we analyzed apoptotic cell death in TNF-treated cpdm MEFs by quantifying the number of cells with active caspase-3. Consistent with previous findings, we observed that TNF treatment for 4 hours markedly increased apoptotic cell death in cpdm MEFs (Fig. 5D). Caspase-3 activation in cpdm MEFs was prevented by restoring SHARPIN expression, but also by increasing PACRG abundance (Fig. 5D). PACRG also prevented apoptosis of SH-SY5Y cells induced by staurosporine (STS) or MPP^+ (1-methyl-4-phenylpyridinium), the active metabolite of the complex I inhibitor MPTP (1-methyl-4-phenyl-1,2,3,6-tetrahydropyridine), similarly to Parkin (fig. S4, A to C). In line with these findings, PACRG silencing increased the vulnerability of SH-SY5Y cells to STS-induced apoptosis (fig. S4D). However, TNF treatment of PACRG-silenced wild-type or cpdm MEFs did not increase caspase-3 activation (fig. S5). This observation suggested a more complex impact of PACRG on cell death regulation that may also affect necroptosis, as has recently been reported for Parkin (*58*).

Impaired NF-κB signaling in the absence of SHARPIN is caused by LUBAC destabilization and increased proteasomal degradation of HOIP (*38*, *48*, *49*). Size exclusion chromatography revealed that HOIP abundance was strongly reduced in cpdm MEFs as compared with wild-type MEFs (fig. S3A). Expression of either SHARPIN or PACRG prevented LUBAC destabilization in cpdm MEFs and restored HOIP abundance to amounts comparable to those detected in wild-type MEFs (fig. S3A). These experiments also confirmed that PACRG was found in high–molecular weight fractions enriched for LUBAC, similarly to SHARPIN (fig. S3A). In addition, we used MEFs to validate a role of PACRG in LUBAC stabilization because we observed that tumor cells were not suitable for this analysis. Reducing PACRG abundance (to about 25% of control conditions) significantly decreased the abundance of HOIP, suggesting an effect on LUBAC stability similar to that of a reduction in SHARPIN (Fig. 5E and fig. S3B). In conclusion, PACRG biochemically and functionally rescued LUBAC stability and activity in SHARPIN-deficient cellular models.

DISCUSSION

In this study, we identified a role for PACRG in TNF-induced NF-κB signaling. In PACRG-silenced cells, NF-κB transcriptional activity, nuclear translocation of p65, degradation of IκBα, and LUBAC-mediated linear ubiquitylation in response to TNF treatment were reduced, which we previously observed for cells in which Parkin had been knocked down or knocked out (*22*). Parkin modifies the LUBAC substrates NEMO and RIPK1 preferentially with K63-linked ubiquitin and, thus, can act as a priming ligase for subsequent M1-linked ubiquitylation by LUBAC (*30*, *33*). PACRG promoted NF-κB signaling in the absence of Parkin, excluding the possibility that it acts by directing Parkin to LUBAC. We found that in response to TNFR1 activation by TNF, PACRG was recruited to the active receptor complex and directly or indirectly interacted with LUBAC. Given that PACRG has no known catalytic activity, the most plausible mode of action was that PACRG acted as an adaptor protein similarly to SHARPIN. In support of a SHARPIN-like role, PACRG rescued defective NF-κB signaling, LUBAC destabilization, and increased susceptibility to TNF-induced cell death in

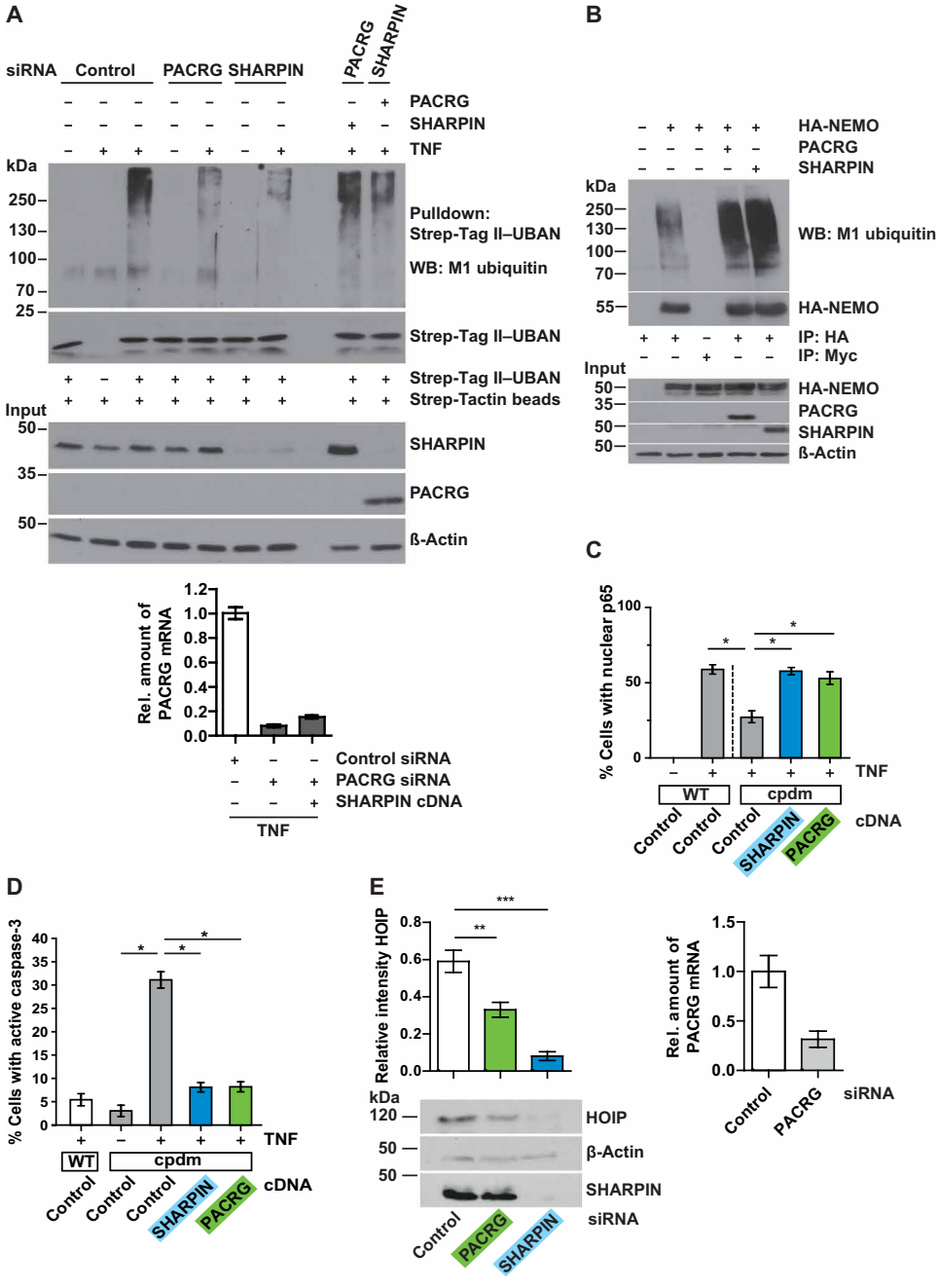

Fig. 5. PACRG restores defective NF-κB activation and prevents increased cell death in SHARPIN-deficient cells. (**A**) HEK293T cells were transfected with control, SHARPIN-, or PACRG-specific siRNAs with or without PACRG or SHARPIN plasmids as indicated, and then the cells were treated with TNF and lysed under denaturing conditions. Linear ubiquitination was analyzed by UBAN affinity purification by Strep-Tag II beads followed by immunoblotting for M1-linked ubiquitin. PACRG knockdown efficiency was determined by real-time RT-PCR. Blot is representative of three independent experiments. (**B**) HEK293T cells were transfected with HA-NEMO and either PACRG or SHARPIN, and then lysed under denaturing conditions followed by immunoprecipitation of NEMO by anti-HA agarose. Anti–c-Myc agarose was used as a control for nonspecific binding. Immunoprecipitated NEMO was immunoblotted for M1-linked ubiquitin and NEMO. The input was immunoblotted for NEMO, PACRG, SHARPIN, and β-actin. Blot is representative of three independent experiments. (**C**) Wild-type (WT) and cpdm MEFs were transfected with SHARPIN, PACRG, or EGFP (negative control), and then the cells were treated with TNF. The fraction of cells showing nuclear translocation of p65 was determined for each condition. Data represent the means ± SEM of three to four independent experiments. For statistical analysis, one-tailed Mann-Whitney *U* test was performed. At least 100 cells were analyzed per condition. (**D**) Cpdm MEFs were transfected with either SHARPIN or PACRG. Transfection of EGFP was used as a control. After TNF treatment, apoptotic cell death was quantified by counting transfected cells positive for active caspase-3. Data represent the means ± SEM of three independent experiments. For statistical analysis one-tailed Mann-Whitney *U* test was performed. At least 100 cells were analyzed per condition. (**E**) MEFs were transiently transfected with the indicated siRNAs and lysed after 48 hours. Lysates were analyzed by immunoblotting for HOIP, SHARPIN, and β-actin. PACRG knockdown efficiency was determined by real-time RT-PCR. Data represent the means ± SEM of five independent experiments; intensity normalized to β-actin is presented as ratio to total intensity of all three bands. For statistical analysis, ANOVA followed by Tukey's multiple comparison test was performed. $*P \leq 0.05$; $**P \leq 0.01$; $***P \leq 0.001$.

SHARPIN-deficient cells. Conversely, SHARPIN rescued decreased TNF-induced linear ubiquitylation in PACRG knockdown cells. These data suggest that SHARPIN and PACRG share partially overlapping functions regarding their ability to act as adaptor proteins for LUBAC.

Whereas SHARPIN harbors the UBD and NZF domains, no functional domains have been identified in PACRG. Thus, SHARPIN and PACRG are likely to have distinct functions that may or may not be LUBAC dependent. For example, SHARPIN can act as an inhibitor of integrin activation (*59*–*61*) and caspase-1 activation (*62*). Moreover, SHARPIN has been described to promote lamellipodium formation by interacting with Arp2/3 (*63*) and to enhance the activity of PRMT5, a type II protein arginine methyltransferase, which contributes to melanomagenesis through the SKI-SOX10 regulatory axis (*64*) in a LUBAC-independent manner.

Concerning the overlapping function of SHARPIN and PACRG in serving as adaptor proteins for LUBAC, an attractive hypothesis would be that functional redundancy might be beneficial regarding the essential role of LUBAC. Loss of HOIP or HOIL-1L in mice causes embryonic lethality (*51*, *65*), whereas SHARPIN KO mice are viable. They suffer from autoinflammation and immunodeficiency due to destabilization of the two remaining LUBAC components

HOIP and HOIL-1L (*38*, *48*, *49*). This phenomenon suggests that at least partial LUBAC activity can be maintained in the absence of SHARPIN, and this might be mediated by PACRG or other adaptor proteins. Thus, it would be interesting to test whether there is a cell type– or tissue-specific increase in *Pacrg* expression or PACRG protein in SHARPIN-deficient mice.

PACRG has mostly been studied in the context of its function in motile cilia; however, a study in *Caenorhabditis elegans* revealed that it also influences signaling pathways regulated by nonmotile primary cilia (*13*). Primary cilia are attracting increasing attention as a hub to regulate and integrate signaling pathways. One of the best-characterized signaling cascades requiring cilia is the sonic hedgehog pathway in vertebrates (*66*, *67*). Recent research indicated a link between NF-κB signaling and cilia. In murine cells with defective ciliogenesis resulting from a hypomorphic mutation in the intraflagellar transport protein ITF88, nuclear translocation of p65 in response to interleukin-1β treatment was impaired due to reduced phosphorylation of IκBα by the IKK complex (*68*). Silencing of the kinesin motor subunit Kif3a, which is required for proper ciliary function, suppressed NF-κB activation in hippocampal neurons treated with lipopolysaccharide (*69*). Moreover, the deubiquitinase CYLD, which hydrolyzes M1- and K63-linked ubiquitin chains and is implicated in regulating TNF signaling, has been linked to the formation of primary cilia (*70*). In this context, increased activation of NF-κB signaling can suppress ciliogenesis, suggesting negative feedback regulation (*71*–*73*). Our study revealed that PACRG acted at the level of LUBAC, which is required to activate the IKK complex. Thus, the regulatory role of PACRG in NF-κB signaling would be compatible with a ciliary function of this protein. Further studies including super-resolution imaging are required to address the question of whether LUBAC components can be recruited to the ciliary compartment.

There is also evidence for a possible role of ciliogenesis and cilia-dependent signaling in PD. Leucine-rich repeat kinase 2 (LRRK2), which is mutated in the majority of autosomal dominant PD and has also been identified as a risk factor for sporadic PD [reviewed in (*74*)], phosphorylates the Rab guanosine triphosphatases (GTPases) Rab8A and Rab10, which regulate ciliogenesis (*75*, *76*). In addition, mutations and polymorphisms in *LRRK2* increase the risk for infections with *Mycobacterium leprae* and are linked to excessive inflammatory responses in leprosy (*77*–*79*).

The functional link between PACRG and Parkin and TNF signaling helps to explain why polymorphisms in the regulatory region of the *PACRG* and *Parkin* genes are well-established susceptibility factors for infections with intracellular pathogens, such as *M. leprae* and *Salmonella* spp. (*18*–*20*, *80*). TNF is an essential cytokine for the control of mycobacterial infections. Mice producing reduced amounts of TNF or mice lacking TNFR1 show increased mortality upon infection with *M. tuberculosis* (*25*). Moreover, mutations in NEMO, a substrate of Parkin, have been linked to Mendelian susceptibility to mycobacterial disease (*81*–*83*). It has recently been shown that LUBAC can modify the surface of cytosolic bacteria with linear ubiquitin chains for local activation of NF-κB and induction of antibacterial autophagy (xenophagy), thereby restricting bacterial proliferation (*84*, *85*). Parkin was found to be recruited to cytosol-invading bacteria (*84*), which may affect both local NF-κB activation and xenophagy. It will be interesting to see whether PACRG is also found in association with cytosolic bacteria and whether intracellular bacteria are localized in proximity to primary cilia. In support of such a scenario, primary cilia are required for the induction of autophagy (*86*). Several key autophagy-related proteins associate with the ciliary axoneme or basal body to promote autophagosome formation in response to cilia-dependent signaling (*87*). In conclusion, our study provides evidence for a role for PACRG in innate immune signaling by interacting with LUBAC and stimulating LUBAC activity.

MATERIALS AND METHODS

Antibodies and reagents

The following antibodies were used: anti-PACRG C8 mouse monoclonal antibody (C-8, sc-37851), anti-Parkin PRK8 mouse monoclonal antibody (PRK8, sc-32282), anti-Hsp60 goat polyclonal antibody (sc-1052), anti-p65 rabbit polyclonal antibody (sc-109) (Santa Cruz Biotechnology), anti–M1-ubiquitin 1E3 rabbit monoclonal antibody (1E3, MABS451) (Millipore), anti–M1-ubiquitin monoclonal 1F11/3F5/Y102L antibody (Genentech), anti–HOIL-1L rabbit polyclonal antibody (ab38540) (Abcam), anti-active caspase-3 rabbit monoclonal antibody (5A1E, 9664), anti-SHARPIN rabbit polyclonal antibody (4444) (Cell Signaling Technology), anti-SHARPIN rabbit polyclonal (14626-1-AP) (Proteintech), anti-IκBα rabbit polyclonal antibody (9242) (Cell Signaling Technology), anti-HA 1.1 mouse monoclonal antibody (16B12, NMS-101R) (Covance), anti–β-actin AC-74 mouse monoclonal antibody (AC-74, A5316), anti-HOIP rabbit polyclonal antibody SAB2102031(Sigma) and A303-560A (Bethyl Laboratories), anti-NEMO rabbit polyclonal antibody (HPA000426) (Sigma), anti-Bax 6A7 mouse monoclonal antibody (eBioscience), ALEXA488 anti-rabbit immunoglobulin G (IgG) (H + L), ALEXA488 anti-mouse IgG heavy and light chain (H + L), ALEXA555 anti-rabbit IgG (H + L), ALEXA555 anti-goat IgG (H + L) (Molecular Probes), horseradish peroxidase (HRP) anti-mouse, anti-rabbit, and anti-goat IgG antibody (Promega), Strep-Tactin HRP conjugate (IBA Lifesciences), anti-HA agarose (mouse), anti–c-Myc agarose (mouse or rabbit), and anti-V5 agarose beads (mouse) (Sigma).

CCCP, bovine serum albumin (BSA), and *N*-ethylenmaleimide were purchased from Sigma, complete protease inhibitor cocktail from Roche, Strep-Tactin sepharose from IBA, TNF from PeproTech (working concentration 25 ng/ml for short-term treatment, 10 ng/ml for 16 hours), FLAG-TNF from ENZO Life Sciences, goat and donkey serum from Cell Signaling Technology, and enhanced chemiluminescence (ECL) reagent from Promega.

Plasmids

The following constructs were described previously: wild-type human-untagged Parkin (*88*), NF-κB–Luc (*30*), HA-HOIP, HA-HOIL-1L, HA-SHARPIN, enhanced green fluorescent protein (EGFP), and UBAN domain from human NEMO (*22*). PACRG cDNA was purified from an RZPD [Deutsches Ressourcenzentrum für Genomforschung (RZPD, Ressourcenzentrum Primärdatenbank)] bacterial clone containing the pCMV-Sport6-PACRG vector and first subcloned into a pCMV vector (vector containing the promotor of cytomegalovirus) by Hind III and Xba I restriction sites. This vector was used for cloning of N-terminally HA-tagged PACRG into the pcDNA3.1(+) vector. The HA tag was amplified with the primers 5′-GCAGAGCTC-GTTTAGTGAACC-3′ (forward) and 5′-TTCTGCCACCAAAA-GAGCGTAATCTG-3′ (reverse). PACRG was amplified using the primers 5′-CAGATTACGCTCTTTTGGTGGCAGAAAAAGAG-3′ (forward) and 5′-GCGAATTCTTAGTTTAGCAAGCAAGCAAG-3′.

Both PCR products were fused together in an additional PCR step. The resulting PCR product and the pcDNA3.1(−) vector were digested with Apa I and Eco RI before ligation. Untagged PACRG was cloned into the pcDNA3.1(+) vector using the In-Fusion cloning strategy provided by Clontech. PACRG was amplified by PCR from the HA-PACRG pcDNA3.1 construct using the following primers: 5′-CAGTGTGGTGGAATTCCCACCATGGTGGCAGAAAAAGAGACCCTG-3′ (forward) and 5′-GATATCTGCAGAATTCTTAGTTTAGCAAGCAAGACTCG-3′ (reverse). The pcDNA3.1(+) vector was linearized with Eco RI restriction enzyme before In-Fusion reaction with the PACRG PCR product. C-terminal HOIP (697 to 1072) was amplified by PCR using the following primers: 5′-TGGAATTCTGCAGATATGCAGGAGTGTGCCGTGTGTGGCTGG-3′ (forward) and 5′-GCCACTGTGCTGGATCTACTTCCGCCTGCGGGGGA-3′ (reverse); N-terminal HOIP (1 to 697) was amplified by PCR using the following primers: 5′-TGGAATTCTGCAGATATGCCGGGGGAGGAAGAGGA-3′ (forward) and 5′- GCCACTGTGCTGGATTTAGGCAAGCAAGCGGCGCAG-3′ (reverse). The pcDNA3.1(+) vector was linearized with Eco RI and Eco RV restriction enzyme before In-Fusion reaction with the HOIP PCR products. The N-terminal HOIP constructs (1 to 298, 1 to 349, 1 to 408, and 1 to 475) were cloned from HA-HOIP in pcDNA3.1(+) with the forward primer 5′-GGAGACCCAAGCTGGCTAGC-3′ and the reverse primer (1 to 298) 5′-ATATTCTAGACTATGCAGGATTAGGGGAAGAAAGAGAGCT-3′, (1 to 349) 5′-ATATTCTAGACTAAAGATCAGGTTCTAGGCCTCCAGTTCC-3′, (1 to 408) 5′-ATATTCTAGACTAGGCAGAGGCCAGCAAAGCAT-3′, and (1 to 475) 5′-ATATTCTAGACTAGCCATGACGATCCAGCCAGGC-3′, respectively. The ΔUBA HOIP mutant was cloned from HA-HOIP in pcDNA3.1(+) by first creating the left and right arms and a subsequent overlap PCR. The primers used were as follows: forward primer left arm 5′-ATATGCGGCCGCATGTACCCATACGATGTTCCAGATTAC-3′, reverse primer left arm 5′-GCGCGCTCTAGACTACTTCCGCCTGCGGGGGATACTC-3′, forward primer right arm 5′-GCAGCAGCAGGCTCGGATCCACTAGTCCAGTGTGGTG-3′, and reverse primer right arm 5′-ATATGAATTCCTTCCGCCTGCGGGGGATAC-3′.

Cell culture, transfection, and RNA interference

SH-SY5Y (DSMZ number ACC 209), HEK293T (CRL-1573; the American Type Culture Collection), Parkin KO MEFs, and HeLa (ACC 57) cells were cultivated as described previously (*22*). SHARPIN KO (cpdm) MEFs and their corresponding wild-type MEFs were cultivated in DMEM supplemented with 10% fetal calf serum and 1% penicillin/streptomycin. Cells were transfected with Lipofectamine/Plus (Invitrogen) according to the manufacturer's instructions. For RNA interference, cells were transfected with the following stealth siRNA oligos (Invitrogen) using Lipofectamine RNAiMAX (Invitrogen): human PACRG siRNA HSS134581/HSS175097/HSS175098, human SHARPIN siRNA HSS149631/HSS149632/HSS188656, mouse PACRG siRNA MSS229626/MSS229627/MSS290650, mouse SHARPIN siRNA MSS272426/MSS272427/MSS272428, and Stealth RNAi siRNA Negative Control Med GC Duplex no. 2 (Invitrogen).

Western blotting

Proteins were size fractionated by SDS–polyacrylamide gel electrophoresis (PAGE) and transferred to nitrocellulose by electroblotting. The nitrocellulose membranes were blocked with 5% nonfat dry milk or 5% BSA in TBST (tris-buffered saline containing 0.1% Tween 20) for 60 min at room temperature and subsequently incubated with the primary antibody diluted in blocking buffer for 16 hours at 4°C. After extensive washing with TBST, the membranes were incubated with HRP-conjugated secondary antibody for 60 min at room temperature. Following washing with TBST, the antigen was detected with the ECL detection system (Promega) as specified by the manufacturer. For quantification of Western blots, Image Studio lite (version 3.1) was used for x-ray films, or AzureSpot (version 2.0) was used for the Sapphire Biomolecular Imager (Azure Biosystems).

Real-time reverse transcription PCR

Total cellular RNA was isolated with the RNeasy Mini Kit (QIAGEN) according to the manufacturer's instructions. cDNA was synthesized using the iScript cDNA Synthesis Kit (Bio-Rad). mRNA quantification was performed with the LightCycler 96 System (Roche) with FastStart Universal SYBR Green Master (Roche), 12 ng of cDNA, and a final primer concentration of 0.5 μM. The following primers were used: human PACRG, 5′-GGTTTCTGAGGGTTTCACAGTC-3′ (forward) and 5′-GGGCTTGGTTGGTCTTTCTT-3′ (reverse); human β-actin, 5′-CCTGGCACCCAGCACAAT-3′ (forward) and 5′-GGGCCGGACTCGTCATAC-3′ (reverse); and mouse HOIP, 5′-CCCAGTGTCACCAGACCTTC-3′ (forward) and 5′-CCTCACAACTCCGTCCTCTG-3′ (reverse).

Apoptosis assay

Activation of caspase-3 was determined by indirect immunofluorescence based on a single-cell analysis. Briefly, cells were grown on glass coverslips. Twenty-four hours after transfection, cells were incubated with TNF (30 ng/ml, 4 hours) or MPP^+ (7.5 μM, 4 hours) or STS (1 μM, 5 hours). The cells were then fixed with 4% paraformaldehyde (PFA) for 10 min, permeabilized with 0.2% Triton X-100 for 10 min, and blocked with 5% goat serum in 0.2% Triton X-100 in phosphate-buffered saline (PBS) for 1 hour at room temperature. Fixed cells were incubated with an antibody against activated caspase-3 overnight at 4°C, followed by an incubation with ALEXA555-conjugated secondary antibody for 1 hour at room temperature. After extensive washing, cells were mounted onto glass slides and analyzed for active caspase-3 by fluorescence microscopy using a Nikon Eclipse E400 microscope.

Nuclear translocation of p65

Translocation of p65 from the cytosol to the nucleus was determined by indirect immunofluorescence based on single-cell analysis. SH-SY5Y cells or MEFs were plated on glass coverslips and transfected with control, PACRG-, or SHARPIN-specific siRNA. Twenty-four hours after transfection, cells were treated with TNF (25 ng/ml) for 20 min and then fixed with 4% PFA in PBS for 10 min at room temperature. Cells were permeabilized with 0.2% Triton X-100 for 10 min and blocked with 5% donkey or goat serum in 0.2% Triton X-100 in PBS for 1 hour at room temperature. Subsequently, cells were incubated with an anti-p65 antibody diluted in blocking buffer overnight at 4°C. After extensive washing, cells were incubated with an ALEXA488-conjugated secondary antibody for 1 hour at room temperature. Last, the cells were washed extensively with PBS and then mounted onto glass slides and analyzed by fluorescence microscopy using a Nikon Eclipse E400 microscope. Nuclei were counterstained with 4′,6-diamidino-2-phenylindole (DAPI) (Sigma), and transfected cells were visualized by mCherry or mitoDsRed plasmid cotransfection. Cells were categorized in

two classes: cells showing complete or incomplete nuclear translocation of p65.

Mitophagy assay

For the analysis of mitophagy, HeLa cells or SH-SY5Y cells overexpressing Parkin, HA-PACRG, and Parkin and HA-PACRG, or silenced for PACRG expression were plated on glass coverslips. Twenty-four hours after transfection, cells were treated with CCCP (10 μM) for 24 hours and then fixed with 4% PFA in PBS for 10 min at room temperature. Cells were permeabilized with 0.2% Triton X-100 for 10 min and blocked with 5% donkey or goat serum in 0.2% Triton X-100 in PBS for 1 hour at room temperature. Subsequently, cells were incubated with an anti-Hsp60 antibody to stain mitochondria, the PRK8 antibody to detect Parkin, or an HA antibody to detect HA-PACRG in blocking buffer overnight at 4°C. After extensive washing, the cells were incubated with an ALEXA488-conjugated and an ALEXA555-conjugated secondary antibody for 1 hour at room temperature. Last, the cells were washed extensively with PBS, mounted onto glass slides, and analyzed by fluorescence microscopy using a Nikon Eclipse E400 microscope. Nuclei were counterstained with DAPI (Sigma).

Luciferase reporter assays

Transfected HEK293T cells or MEFs were lysed in reporter lysis buffer (Promega) 16 hours after TNF treatment (10 ng/ml) or 1 day after cotransfection of HEK293T cells or 2 days after cotransfection of MEFs. Lysates were cleared by centrifugation, and luciferase activity was determined luminometrically (TriStar^2 LB 942, Berthold Technologies) by the luciferase assay system (Promega). The measured values were normalized to protein levels. Quantifications were based on at least three independent experiments, each performed in triplicate.

Coimmunoprecipitation experiments

Untransfected HEK293T cells or HEK293T cells transfected with the indicated constructs were lysed in lysis buffer (1% Triton X-100 in PBS and protease inhibitor). The lysates were cleared by centrifugation (20,000*g* for 20 min) and incubated overnight at 4°C with the antibody indicated coupled to agarose beads. To control for unspecific binding to either agarose beads or immunoglobulin, anti–c-Myc agarose beads were used in comparison to anti-HA agarose beads. After washing three times with lysis buffer, Laemmli sample buffer was added, and the samples were boiled for 10 min.

Isolation of the active TNFR1 signaling complex

HEK293T cells were incubated with FLAG-TNF (500 ng/ml) (Enzo Life Sciences) for the indicated time 24 hours after transfection. Subsequently, cells were lysed in lysis buffer (1% Triton X-100 in PBS and protease inhibitor, 10 μM *N*-ethylmaleimide), incubated on ice for 5 min, and centrifuged at 20,000*g* for 20 min. Twenty microliters of protein A agarose beads preincubated with anti-FLAG antibody was added to the supernatant and incubated overnight at 4°C. After washing three times with lysis buffer, Laemmli sample buffer was added, and the samples were boiled for 10 min.

Linear ubiquitylation assay

HEK293T cells transfected with the indicated constructs and treated with or without TNF (25 ng/ml, 15 or 30 min) were lysed in denaturing lysis buffer (1% SDS in PBS) and incubated at 95°C for 30 min. Protein extracts were diluted 1:10 with nondenaturing lysis buffer (1% Triton X-100 in PBS) and cleared by centrifugation. To pull down proteins modified by linear ubiquitin chains, 20 μg of the recombinant UBAN domain of NEMO was added, which carries an N-terminal Strep-Tag II. After incubation for 1 hour at 4°C, Strep-Tactin beads were added and incubated overnight at 4°C. Beads were collected by centrifugation and washed. Laemmli sample buffer was added, and the samples were boiled for 10 min. Proteins binding to the UBAN domain were separated with SDS-PAGE and analyzed by Western blotting using an anti–M1-ubiquitin antibody.

HOIP protein abundance in MEFs silenced for PACRG or SHARPIN expression

MEFs were grown on 10-cm dishes and transiently transfected with control, SHARPIN-, or PACRG-specific siRNAs. After 48 hours, cells were lysed in 1% Triton X-100 (v/v) in PBS with protease inhibitors and heated to 95°C for 10 min with 5× Laemmli sample buffer. Samples were analyzed by immunoblotting using antibodies against HOIP (Bethyl Laboratories), SHARPIN (Proteintech), and β-actin.

Protein expression and purification

Recombinant proteins were produced in *Escherichia coli* strain BL21DE3 using the pIBA3plus expression system (IBA). Bacteria were grown to a density of an absorbance at a wavelength of 600 nm (A_{600}) value of 0.6 to 0.8, and protein expression was induced by anhydrotetracycline (200 ng/ml) (IBA). After culturing bacteria for 3 hours at 37°C, cultures were harvested by centrifugation at 3000*g*, and pellets were resuspended in lysis buffer [100 mM tris (pH 8.0), 150 mM NaCl, and protease inhibitors) at 4°C. Subsequently, cells were lysed by sheering forces using a French press and afterward centrifuged for 60 min at 40,000*g* (4°C) to get rid of cellular debris. Bacterial lysates containing the Strep-tagged UBAN domain were loaded on a StrepTrap column (GE Healthcare) and washed with 100 mM tris (pH 8.0) and 150 mM NaCl. After washing, the UBAN domain was eluted with 100 mM tris-HCl (pH 8.0), 150 mM NaCl, and 2.5 mM D-desthiobiotin. Eluted fractions containing the protein were pooled and concentrated using Amicon Ultra-15 spin columns (Millipore) with an exclusion size of 10 kDa.

Size-exclusion chromatography

MEFs expressing either SHARPIN or PACRG were lysed in a tris buffer [50 mM tris (pH 7.5), 1 mM $MgCl_2$, 1 mM dithiothreitol, and complete protease inhibitor) by repeated passing through a syringe needle. After 15 min of incubation on ice, lysates were cleared by centrifugation (20,000*g*, 20 min, 4°C). Protein concentration of the samples was measured by the Bradford protein assay, and equal amounts of proteins were loaded on the column. Proteins were separated on a Superdex 200 10/300 GL column using an ÄKTA chromatography system (GE Healthcare Life Sciences). Fractions [0.5 ml (fig. S1) or 1 ml (fig. S3A)] were collected and analyzed by Western blotting using antibodies against HOIP, SHARPIN, or PACRG. All blots corresponding to fig. S3A were exposed to a single x-ray film so that exposure time was the same.

Statistical analysis

Data represent the means ± SD or SEM from $n \geq 3$ biological replicates (indicated in the figure legends). All statistical analyses were performed by using GraphPad Prism (version 5; San Diego, CA, USA). To check the normal distribution of data, the Kolmogorov-Smirnov

test was applied. On the basis of the outcome of the test, appropriate parametric and nonparametric tests were chosen. For the comparison of two independent parametric datasets, Student's *t* test was used. For the comparison of more than two parametric datasets, one-way analysis of variance (ANOVA) was applied. To correct for α-error inflation resulting from multiple comparisons, ANOVA was followed by Tukey's post hoc multiple comparison tests. For the direct comparison of two nonparametric datasets, Wilcoxon–Mann-Whitney (*U* test) was used. Statistical significance levels for all tests: $*P \leq 0.05$; $**P \leq 0.01$; $***P \leq 0.001$.

SUPPLEMENTARY MATERIALS

stke.sciencemag.org/cgi/content/full/13/617/eaav1256/DC1
Fig. S1. PACRG coelutes with endogenous LUBAC components.
Fig. S2. PACRG restores defective p65 translocation in SHARPIN-deficient cells.
Fig. S3. PACRG stabilizes LUBAC.
Fig. S4. PACRG protects against STS- and MPP^+-induced apoptotic cell death.
Fig. S5. TNF treatment of PACRG-silenced MEFs does not activate caspase-3.
Table S1. Antibodies used in this study.

View/request a protocol for this paper from *Bio-protocol*.

REFERENCES AND NOTES

1. A. B. West, P. J. Lockhart, C. O'Farell, M. J. Farrer, Identification of a novel gene linked to parkin via a bi-directional promoter. *J. Mol. Biol.* **326**, 11–19 (2003).
2. A. M. Pickrell, R. J. Youle, The roles of PINK1, parkin, and mitochondrial fidelity in Parkinson's disease. *Neuron* **85**, 257–273 (2015).
3. A. J. Whitworth, L. J. Pallanck, PINK1/Parkin mitophagy and neurodegeneration—What do we really know in vivo? *Curr. Opin. Genet. Dev.* **44**, 47–53 (2017).
4. T. N. Nguyen, B. S. Padman, M. Lazarou, Deciphering the molecular signals of PINK1/Parkin mitophagy. *Trends Cell Biol.* **26**, 733–744 (2016).
5. T. G. McWilliams, M. M. K. Muqit, PINK1 and Parkin: Emerging themes in mitochondrial homeostasis. *Curr. Opin. Cell Biol.* **45**, 83–91 (2017).
6. L. A. Scarffe, D. A. Stevens, V. L. Dawson, T. M. Dawson, Parkin and PINK1: Much more than mitophagy. *Trends Neurosci.* **37**, 315–324 (2014).
7. K. F. Winklhofer, Parkin and mitochondrial quality control: Toward assembling the puzzle. *Trends Cell Biol.* **24**, 332–341 (2014).
8. L. Scott, V. L. Dawson, T. M. Dawson, Trumping neurodegeneration: Targeting common pathways regulated by autosomal recessive Parkinson's disease genes. *Exp. Neurol.* **298**, 191–201 (2017).
9. Z. Zhang, X. Shen, D. R. Gude, B. M. Wilkinson, M. J. Justice, C. J. Flickinger, J. C. Herr, E. M. Eddy, J. F. Strauss III, MEIG1 is essential for spermiogenesis in mice. *Proc. Natl. Acad. Sci. U.S.A.* **106**, 17055–17060 (2009).
10. W. Li, W. Tang, M. E. Teves, Z. Zhang, L. Zhang, H. Li, K. J. Archer, D. L. Peterson, D. C. Williams Jr., J. F. Strauss III, Z. Zhang, A MEIG1/PACRG complex in the manchette is essential for building the sperm flagella. *Development* **142**, 921–930 (2015).
11. D. Lorenzetti, C. E. Bishop, M. J. Justice, Deletion of the Parkin coregulated gene causes male sterility in the *quaking*^{viable} mouse mutant. *Proc. Natl. Acad. Sci. U.S.A.* **101**, 8402–8407 (2004).
12. G. R. Wilson, H. X. Wang, G. F. Egan, P. J. Robinson, M. B. Delatycki, M. K. O'Bryan, P. J. Lockhart, Deletion of the Parkin co-regulated gene causes defects in ependymal ciliary motility and hydrocephalus in the quakingviable mutant mouse. *Hum. Mol. Genet.* **19**, 1593–1602 (2010).
13. C. M. Loucks, N. J. Bialas, M. P. Dekkers, D. S. Walker, L. J. Grundy, C. Li, P. N. Inglis, K. Kida, W. R. Schafer, O. E. Blacque, G. Jansen, M. R. Leroux, PACRG, a protein linked to ciliary motility, mediates cellular signaling. *Mol. Biol. Cell* **27**, 2133–2144 (2016).
14. S. E. M. Stephenson, T. D. Aumann, J. M. Taylor, J. R. Riseley, R. Li, J. R. Mann, D. Tomas, P. J. Lockhart, Generation and characterisation of a *parkin-Pacrg* knockout mouse line and a Pacrg knockout mouse line. *Sci. Rep.* **8**, 7528 (2018).
15. Y. Imai, M. Soda, T. Murakami, M. Shoji, K. Abe, R. Takahashi, A product of the human gene adjacent to *parkin* is a component of Lewy bodies and suppresses Pael receptor-induced cell death. *J. Biol. Chem.* **278**, 51901–51910 (2003).
16. J. M. Taylor, Y. J. Song, Y. Huang, M. J. Farrer, M. B. Delatycki, G. M. Halliday, P. J. Lockhart, Parkin Co-Regulated Gene (PACRG) is regulated by the ubiquitin-proteasomal system and is present in the pathological features of Parkinsonian diseases. *Neurobiol. Dis.* **27**, 238–247 (2007).
17. Y. Imai, M. Soda, H. Inoue, N. Hattori, Y. Mizuno, R. Takahashi, An unfolded putative transmembrane polypeptide, which can lead to endoplasmic reticulum stress, is a substrate of parkin. *Cell* **105**, 891–902 (2001).
18. M. T. Mira, A. Alcaïs, V. T. Nguyen, M. O. Moraes, C. Di Flumeri, H. T. Vu, C. P. Mai, T. H. Nguyen, N. B. Nguyen, X. K. Pham, E. N. Sarno, A. Alter, A. Montpetit, M. E. Moraes, J. R. Moraes, C. Dore, C. J. Gallant, P. Lepage, A. Verner, E. van de Vosse, T. J. Hudson, L. Abel, E. Schurr, Susceptibility to leprosy is associated with PARK2 and PACRG. *Nature* **427**, 636–640 (2004).
19. S. Ali, A. M. Vollaard, S. Widjaja, C. Surjadi, E. van de Vosse, J. T. van Dissel, PARK2/PACRG polymorphisms and susceptibility to typhoid and paratyphoid fever. *Clin. Exp. Immunol.* **144**, 425–431 (2006).
20. A. Alter, V. M. Fava, N. T. Huong, M. Singh, M. Orlova, N. Van Thuc, K. Katoch, V. H. Thai, N. N. Ba, L. Abel, N. Mehra, A. Alcais, E. Schurr, Linkage disequilibrium pattern and age-at-diagnosis are critical for replicating genetic associations across ethnic groups in leprosy. *Hum. Genet.* **132**, 107–116 (2013).
21. R. Chopra, S. Ali, A. K. Srivastava, S. Aggarwal, B. Kumar, S. Manvati, P. Kalaiarasan, M. Jena, V. K. Garg, S. N. Bhattacharya, R. N. K. Bamezai, Mapping of PARK2 and PACRG overlapping regulatory region reveals LD structure and functional variants in association with leprosy in unrelated Indian population groups. *PLOS Genet.* **9**, e1003578 (2013).
22. A. K. Muller-Rischart, A. Pilsl, P. Beaudette, M. Patra, K. Hadian, M. Funke, R. Peis, A. Deinlein, C. Schweimer, P. H. Kuhn, S. F. Lichtenthaler, E. Motori, S. Hrelia, W. Wurst, D. Trumbach, T. Langer, D. Krappmann, G. Dittmar, J. Tatzelt, K. F. Winklhofer, The E3 ligase parkin maintains mitochondrial integrity by increasing linear ubiquitination of NEMO. *Mol. Cell* **49**, 908–921 (2013).
23. Y.-Y. Li, H. Yu, Z.-M. Guo, T.-Q. Guo, K. Tu, Y.-X. Li, Systematic analysis of head-to-head gene organization: Evolutionary conservation and potential biological relevance. *PLOS Comput. Biol.* **2**, e74 (2006).
24. N. Ramirez-Alejo, L. Santos-Argumedo, Innate defects of the IL-12/IFN-gamma axis in susceptibility to infections by mycobacteria and *Salmonella*. *J. Interferon Cytokine Res.* **34**, 307–317 (2014).
25. J. L. Flynn, M. M. Goldstein, J. Chan, K. J. Triebold, K. Pfeffer, C. J. Lowenstein, R. Schreiber, T. W. Mak, B. R. Bloom, Tumor necrosis factor-α is required in the protective immune response against Mycobacterium tuberculosis in mice. *Immunity* **2**, 561–572 (1995).
26. A. Dorhoi, S. H. E. Kaufmann, Tumor necrosis factor alpha in mycobacterial infection. *Semin. Immunol.* **26**, 203–209 (2014).
27. D. Narendra, A. Tanaka, D.-F. Suen, R. J. Youle, Parkin is recruited selectively to impaired mitochondria and promotes their autophagy. *J. Cell Biol.* **183**, 795–803 (2008).
28. S. Geisler, K. M. Holmström, D. Skujat, F. C. Fiesel, O. C. Rothfuss, P. J. Kahle, W. Springer, PINK1/Parkin-mediated mitophagy is dependent on VDAC1 and p62/SQSTM1. *Nat. Cell Biol.* **12**, 119–131 (2010).
29. S. R. Denison, F. Wang, N. A. Becker, B. Schule, N. Kock, L. A. Phillips, C. Klein, D. I. Smith, Alterations in the common fragile site gene Parkin in ovarian and other cancers. *Oncogene* **22**, 8370–8378 (2003).
30. I. H. Henn, L. Bouman, J. S. Schlehe, A. Schlierf, J. E. Schramm, E. Wegener, K. Nakaso, C. Culmsee, B. Berninger, D. Krappmann, J. Tatzelt, K. F. Winklhofer, Parkin mediates neuroprotection through activation of IκB kinase/nuclear factor-κB signaling. *J. Neurosci.* **27**, 1868–1878 (2007).
31. D. Sha, L.-S. Chin, L. Li, Phosphorylation of parkin by Parkinson disease-linked kinase PINK1 activates parkin E3 ligase function and NF-κB signaling. *Hum. Mol. Genet.* **19**, 352–363 (2010).
32. D. P. Meka, A. K. Müller-Rischart, P. Nidadavolu, B. Mohammadi, E. Motori, S. K. Ponna, H. Aboutalebi, M. Bassal, A. Annamneedi, B. Finckh, M. Miesbauer, N. Rotermund, C. Lohr, J. Tatzelt, K. F. Winklhofer, E. R. Kramer, Parkin cooperates with GDNF/RET signaling to prevent dopaminergic neuron degeneration. *J. Clin. Invest.* **125**, 1873–1885 (2015).
33. Y. Wang, B. Shan, Y. Liang, H. Wei, J. Yuan, Parkin regulates NF-κB by mediating site-specific ubiquitination of RIPK1. *Cell Death Dis.* **9**, 732 (2018).
34. T. L. Haas, C. H. Emmerich, B. Gerlach, A. C. Schmukle, S. M. Cordier, E. Rieser, R. Feltham, J. Vince, U. Warnken, T. Wenger, R. Koschny, D. Komander, J. Silke, H. Walczak, Recruitment of the linear ubiquitin chain assembly complex stabilizes the TNF-R1 signaling complex and is required for TNF-mediated gene induction. *Mol. Cell* **36**, 831–844 (2009).
35. F. Tokunaga, S.-i. Sakata, Y. Saeki, Y. Satomi, T. Kirisako, K. Kamei, T. Nakagawa, M. Kato, S. Murata, S. Yamaoka, M. Yamamoto, S. Akira, T. Takao, K. Tanaka, K. Iwai, Involvement of linear polyubiquitylation of NEMO in NF-κB activation. *Nat. Cell Biol.* **11**, 123–132 (2009).
36. M. Hrdinka, M. Gyrd-Hansen, The Met1-linked ubiquitin machinery: Emerging themes of (de)regulation. *Mol. Cell* **68**, 265–280 (2017).
37. K. Rittinger, F. Ikeda, Linear ubiquitin chains: Enzymes, mechanisms and biology. *Open Biol.* **7**, 170026 (2017).
38. B. Gerlach, S. M. Cordier, A. C. Schmukle, C. H. Emmerich, E. Rieser, T. L. Haas, A. I. Webb, J. A. Rickard, H. Anderton, W. W.-L. Wong, U. Nachbur, L. Gangoda, U. Warnken, A. W. Purcell, J. Silke, H. Walczak, Linear ubiquitination prevents inflammation and regulates immune signalling. *Nature* **471**, 591–596 (2011).
39. J. J. Smit, D. Monteferrario, S. M. Noordermeer, W. J. van Dijk, B. A. van der Reijden, T. K. Sixma, The E3 ligase HOIP specifies linear ubiquitin chain assembly through its RING-IBR-RING domain and the unique LDD extension. *EMBO J.* **31**, 3833–3844 (2012).

40. P. Draber, S. Kupka, M. Reichert, H. Draberova, E. Lafont, D. de Miguel, L. Spilgies, S. Surinova, L. Taraborrelli, T. Hartwig, E. Rieser, L. Martino, K. Rittinger, H. Walczak, LUBAC-recruited CYLD and A20 regulate gene activation and cell death by exerting opposing effects on linear ubiquitin in signaling complexes. *Cell Rep.* **13**, 2258–2272 (2015).
41. C. H. Emmerich, A. Ordureau, S. Strickson, J. S. C. Arthur, P. G. A. Pedrioli, D. Komander, P. Cohen, Activation of the canonical IKK complex by K63/M1-linked hybrid ubiquitin chains. *Proc. Natl. Acad. Sci. U.S.A.* **110**, 15247–15252 (2013).
42. M. Hrdinka, B. K. Fiil, M. Zucca, D. Leske, K. Bagola, M. Yabal, P. R. Elliott, R. B. Damgaard, D. Komander, P. J. Jost, M. Gyrd-Hansen, CYLD limits Lys63- and Met1-linked ubiquitin at receptor complexes to regulate innate immune signaling. *Cell Rep.* **14**, 2846–2858 (2016).
43. B. K. Fiil, R. B. Damgaard, S. A. Wagner, K. Keusekotten, M. Fritsch, S. Bekker-Jensen, N. Mailand, C. Choudhary, D. Komander, M. Gyrd-Hansen, OTULIN restricts Met1-linked ubiquitination to control innate immune signaling. *Mol. Cell* **50**, 818–830 (2013).
44. S. Rahighi, F. Ikeda, M. Kawasaki, M. Akutsu, N. Suzuki, R. Kato, T. Kensche, T. Uejima, S. Bloor, D. Komander, F. Randow, S. Wakatsuki, I. Dikic, Specific recognition of linear ubiquitin chains by NEMO is important for NF-κB activation. *Cell* **136**, 1098–1109 (2009).
45. D. Komander, F. Reyes-Turcu, J. D. F. Licchesi, P. Odenwaelder, K. D. Wilkinson, D. Barford, Molecular discrimination of structurally equivalent Lys 63-linked and linear polyubiquitin chains. *EMBO Rep.* **10**, 466–473 (2009).
46. K. Hadian, R. A. Griesbach, S. Dornauer, T. M. Wanger, D. Nagel, M. Metlitzky, W. Beisker, M. Schmidt-Supprian, D. Krappmann, NF-κB Essential Modulator (NEMO) interaction with linear and Lys-63 ubiquitin chains contributes to NF-κB activation. *J. Biol. Chem.* **286**, 26107–26117 (2011).
47. M. L. Matsumoto, K. C. Dong, C. Yu, L. Phu, X. Gao, R. N. Hannoush, S. G. Hymowitz, D. S. Kirkpatrick, V. M. Dixit, R. F. Kelley, Engineering and structural characterization of a linear polyubiquitin-specific antibody. *J. Mol. Biol.* **418**, 134–144 (2012).
48. F. Ikeda, Y. L. Deribe, S. S. Skånland, B. Stieglitz, C. Grabbe, M. Franz-Wachtel, S. J. L. van Wijk, P. Goswami, V. Nagy, J. Terzic, F. Tokunaga, A. Androulidaki, T. Nakagawa, M. Pasparakis, K. Iwai, J. P. Sundberg, L. Schaefer, K. Rittinger, B. Macek, I. Dikic, SHARPIN forms a linear ubiquitin ligase complex regulating NF-κB activity and apoptosis. *Nature* **471**, 637–641 (2011).
49. F. Tokunaga, T. Nakagawa, M. Nakahara, Y. Saeki, M. Taniguchi, S.-i. Sakata, K. Tanaka, H. Nakano, K. Iwai, SHARPIN is a component of the NF-κB-activating linear ubiquitin chain assembly complex. *Nature* **471**, 633–636 (2011).
50. J. Liu, Y. Wang, Y. Gong, T. Fu, S. Hu, Z. Zhou, L. Pan, Structural insights into SHARPIN-mediated activation of HOIP for the linear ubiquitin chain assembly. *Cell Rep.* **21**, 27–36 (2017).
51. H. Fujita, A. Tokunaga, S. Shimizu, A. L. Whiting, F. Aguilar-Alonso, K. Takagi, E. Walinda, Y. Sasaki, T. Shimokawa, T. Mizushima, I. Ohki, M. Ariyoshi, H. Tochio, F. Bernal, M. Shirakawa, K. Iwai, Cooperative domain formation by homologous motifs in HOIL-1L and SHARPIN plays a crucial role in LUBAC stabilization. *Cell Rep.* **23**, 1192–1204 (2018).
52. B. Stieglitz, A. C. Morris-Davies, M. G. Koliopoulos, E. Christodoulou, K. Rittinger, LUBAC synthesizes linear ubiquitin chains via a thioester intermediate. *EMBO Rep.* **13**, 840–846 (2012).
53. H. Yagi, K. Ishimoto, T. Hiromoto, H. Fujita, T. Mizushima, Y. Uekusa, M. Yagi-Utsumi, E. Kurimoto, M. Noda, S. Uchiyama, F. Tokunaga, K. Iwai, K. Kato, A non-canonical UBA-UBL interaction forms the linear-ubiquitin-chain assembly complex. *EMBO Rep.* **13**, 462–468 (2012).
54. B. Stieglitz, R. R. Rana, M. G. Koliopoulos, A. C. Morris-Davies, V. Schaeffer, E. Christodoulou, S. Howell, N. R. Brown, I. Dikic, K. Rittinger, Structural basis for ligase-specific conjugation of linear ubiquitin chains by HOIP. *Nature* **503**, 422–426 (2013).
55. R. E. Seymour, M. G. Hasham, G. A. Cox, L. D. Shultz, H. Hogenesch, D. C. Roopenian, J. P. Sundberg, Spontaneous mutations in the mouse Sharpin gene result in multiorgan inflammation, immune system dysregulation and dermatitis. *Genes Immun.* **8**, 416–421 (2007).
56. J. A. Rickard, H. Anderton, N. Etemadi, U. Nachbur, M. Darding, N. Peltzer, N. Lalaoui, K. E. Lawlor, H. Vanyai, C. Hall, A. Bankovacki, L. Gangoda, W. W. Wong, J. Corbin, C. Huang, E. S. Mocarski, J. M. Murphy, W. S. Alexander, A. K. Voss, D. L. Vaux, W. J. Kaiser, H. Walczak, J. Silke, TNFR1-dependent cell death drives inflammation in Sharpin-deficient mice. *eLife* **3**, e03464 (2014).
57. S. Kumari, Y. Redouane, J. Lopez-Mosqueda, R. Shiraishi, M. Romanowska, S. Lutzmayer, J. Kuiper, C. Martinez, I. Dikic, M. Pasparakis, F. Ikeda, Sharpin prevents skin inflammation by inhibiting TNFR1-induced keratinocyte apoptosis. *eLife* **3**, e03422 (2014).
58. S. B. Lee, J. J. Kim, S.-A. Han, Y. Fan, L.-S. Guo, K. Aziz, S. Nowsheen, S. S. Kim, S.-Y. Park, Q. Luo, J. O. Chung, S. I. Choi, A. Aziz, P. Yin, S.-Y. Tong, F. C. Fiesel, W. Springer, J.-S. Zhang, Z. Lou, The AMPK-Parkin axis negatively regulates necroptosis and tumorigenesis by inhibiting the necrosome. *Nat. Cell Biol.* **21**, 940–951 (2019).
59. J. K. Rantala, J. Pouwels, T. Pellinen, S. Veltel, P. Laasola, E. Mattila, C. S. Potter, T. Duffy, J. P. Sundberg, O. Kallioniemi, J. A. Askari, M. J. Humphries, M. Parsons, M. Salmi, J. Ivaska, SHARPIN is an endogenous inhibitor of beta1-integrin activation. *Nat. Cell Biol.* **13**, 1315–1324 (2011).
60. J. Pouwels, N. De Franceschi, P. Rantakari, K. Auvinen, M. Karikoski, E. Mattila, C. Potter, J. P. Sundberg, N. Hogg, C. G. Gahmberg, M. Salmi, J. Ivaska, SHARPIN regulates uropod detachment in migrating lymphocytes. *Cell Rep.* **5**, 619–628 (2013).
61. N. De Franceschi, E. Peuhu, M. Parsons, S. Rissanen, I. Vattulainen, M. Salmi, J. Ivaska, J. Pouwels, Mutually exclusive roles of SHARPIN in integrin inactivation and NF-κB signaling. *PLOS ONE* **10**, e0143423 (2015).
62. M.-V. Nastase, J. Zeng-Brouwers, H. Frey, L. T. Hsieh, C. Poluzzi, J. Beckmann, N. Schroeder, J. Pfeilschifter, J. Lopez-Mosqueda, J. Mersmann, F. Ikeda, R. V. Iozzo, I. Dikic, L. Schaefer, An essential role for SHARPIN in the regulation of caspase 1 activity in sepsis. *Am. J. Pathol.* **186**, 1206–1220 (2016).
63. M. H. Khan, S. I. Salomaa, G. Jacquemet, U. Butt, M. Miihkinen, T. Deguchi, E. Kremneva, P. Lappalainen, M. J. Humphries, J. Pouwels, The Sharpin interactome reveals a role for Sharpin in lamellipodium formation via the Arp2/3 complex. *J. Cell Sci.* **130**, 3094–3107 (2017).
64. H. Tamiya, H. Kim, O. Klymenko, H. Kim, Y. Feng, T. Zhang, J. Y. Han, A. Murao, S. J. Snipas, L. Jilaveanu, K. Brown, H. Kluger, H. Zhang, K. Iwai, Z. A. Ronai, SHARPIN-mediated regulation of protein arginine methyltransferase 5 controls melanoma growth. *J. Clin. Invest.* **128**, 517–530 (2018).
65. N. Peltzer, E. Rieser, L. Taraborrelli, P. Draber, M. Darding, B. Pernaute, Y. Shimizu, A. Sarr, H. Draberova, A. Montinaro, J. P. Martinez-Barbera, J. Silke, T. A. Rodriguez, H. Walczak, HOIP deficiency causes embryonic lethality by aberrant TNFR1-mediated endothelial cell death. *Cell Rep.* **9**, 153–165 (2014).
66. R. Rohatgi, L. Milenkovic, M. P. Scott, Patched1 regulates hedgehog signaling at the primary cilium. *Science* **317**, 372–376 (2007).
67. K. C. Corbit, P. Aanstad, V. Singla, A. R. Norman, D. Y. R. Stainier, J. F. Reiter, Vertebrate Smoothened functions at the primary cilium. *Nature* **437**, 1018–1021 (2005).
68. A. K. T. Wann, J. P. Chapple, M. M. Knight, The primary cilium influences interleukin-1β-induced NFκB signalling by regulating IKK activity. *Cell. Signal.* **26**, 1735–1742 (2014).
69. H. Baek, H. J. Shin, J.-J. Kim, N. Shin, S. Kim, M.-H. Yi, E. Zhang, J. Hong, J. W. Kang, Y. Kim, C. S. Kim, D. W. Kim, Primary cilia modulate TLR4-mediated inflammatory responses in hippocampal neurons. *J. Neuroinflammation* **14**, 189 (2017).
70. T. Eguether, M. A. Ermolaeva, Y. Zhao, M. C. Bonnet, A. Jain, M. Pasparakis, G. Courtois, A.-M. Tassin, The deubiquitinating enzyme CYLD controls apical docking of basal bodies in ciliated epithelial cells. *Nat. Commun.* **5**, 4585 (2014).
71. A. Vezina, E. Vaillancourt-Jean, S. Albarao, B. Annabi, Mesenchymal stromal cell ciliogenesis is abrogated in response to tumor necrosis factor-α and requires NF-κB signaling. *Cancer Lett.* **345**, 100–105 (2014).
72. M. Lattke, A. Magnutzki, P. Walther, T. Wirth, B. Baumann, Nuclear factor κB activation impairs ependymal ciliogenesis and links neuroinflammation to hydrocephalus formation. *J. Neurosci.* **32**, 11511–11523 (2012).
73. C. Huber, S. Wu, A. S. Kim, S. Sigaudy, A. Sarukhanov, V. Serre, G. Baujat, K.-H. Le Quan Sang, D. L. Rimoin, D. H. Cohn, A. Munnich, D. Krakow, V. Cormier-Daire, WDR34 mutations that cause short-rib polydactyly syndrome type III/severe asphyxiating thoracic dysplasia reveal a role for the NF-κB pathway in cilia. *Am. J. Hum. Genet.* **93**, 926–931 (2013).
74. J. H. Kluss, A. Mamais, M. R. Cookson, LRRK2 links genetic and sporadic Parkinson's disease. *Biochem. Soc. Trans.* **47**, 651–661 (2019).
75. H. S. Dhekne, I. Yanatori, R. C. Gomez, F. Tonelli, F. Diez, B. Schule, M. Steger, D. R. Alessi, S. R. Pfeffer, A pathway for Parkinson's Disease LRRK2 kinase to block primary cilia and Sonic hedgehog signaling in the brain. *eLife* **7**, e40202 (2018).
76. M. Steger, F. Diez, H. S. Dhekne, P. Lis, R. S. Nirujogi, O. Karayel, F. Tonelli, T. N. Martinez, E. Lorentzen, S. R. Pfeffer, D. R. Alessi, M. Mann, Systematic proteomic analysis of LRRK2-mediated Rab GTPase phosphorylation establishes a connection to ciliogenesis. *eLife* **6**, e31012 (2017).
77. V. M. Fava, J. Manry, A. Cobat, M. Orlova, N. Van Thuc, N. N. Ba, V. H. Thai, L. Abel, A. Alcaïs, E. Schurr; Canadian Lrrk2 in Inflammation Team (CLINT), A missense LRRK2 variant is a risk factor for excessive inflammatory responses in leprosy. *PLOS Negl Trop Dis.* **10**, e0004412 (2016).
78. F.-R. Zhang, W. Huang, S.-M. Chen, L.-D. Sun, H. Liu, Y. Li, Y. Cui, X.-X. Yan, H.-T. Yang, R.-D. Yang, T.-S. Chu, C. Zhang, L. Zhang, J.-W. Han, G.-Q. Yu, C. Quan, Y.-X. Yu, Z. Zhang, B.-Q. Shi, L.-H. Zhang, H. Cheng, C.-Y. Wang, Y. Lin, H.-F. Zheng, X.-A. Fu, X.-B. Zuo, Q. Wang, H. Long, Y.-P. Sun, Y.-L. Cheng, H.-Q. Tian, F.-S. Zhou, H.-X. Liu, W.-S. Lu, S.-M. He, W.-L. Du, M. Shen, Q.-Y. Jin, Y. Wang, H.-Q. Low, T. Erwin, N.-H. Yang, J.-Y. Li, X. Zhao, Y.-L. Jiao, L. G. Mao, G. Yin, Z.-X. Jiang, X.-D. Wang, J.-P. Yu, Z.-H. Hu, C.-H. Gong, Y.-Q. Liu, R.-Y. Liu, D.-M. Wang, D. Wei, J.-X. Liu, W.-K. Cao, H.-Z. Cao, Y.-P. Li, W.-G. Yan, S.-Y. Wei, K.-J. Wang, M. L. Hibberd, S. Yang, X.-J. Zhang, J.-J. Liu, Genomewide association study of leprosy. *N. Engl. J. Med.* **361**, 2609–2618 (2009).
79. V. M. Fava, Y. Z. Xu, G. Lettre, N. Van Thuc, M. Orlova, V. H. Thai, S. Tao, N. Croteau, M. A. Eldeeb, E. J. MacDougall, G. Cambri, R. Lahiri, L. Adams, E. A. Fon, J.-F. Trempe, A. Cobat, A. Alcaïs, L. Abel, E. Schurr, Pleiotropic effects for Parkin and LRRK2 in leprosy type-1 reactions and Parkinson's disease. *Proc. Natl. Acad. Sci. U.S.A.* **116**, 15616–15624 (2019).
80. G. Cambri, M. T. Mira, Genetic susceptibility to leprosy—From classic immune-related candidate genes to hypothesis-free, whole genome approaches. *Front. Immunol.* **9**, 1674 (2018).

81. O. Filipe-Santos, J. Bustamante, M. H. Haverkamp, E. Vinolo, C.-L. Ku, A. Puel, D. M. Frucht, K. Christel, H. von Bernuth, E. Jouanguy, J. Feinberg, A. Durandy, B. Senechal, A. Chapgier, G. Vogt, L. de Beaucoudrey, C. Fieschi, C. Picard, M. Garfa, J. Chemli, M. Bejaoui, M. N. Tsolia, N. Kutukculer, A. Plebani, L. Notarangelo, C. Bodemer, F. Geissmann, A. Israel, M. Veron, M. Knackstedt, R. Barbouche, L. Abel, K. Magdorf, D. Gendrel, F. Agou, S. M. Holland, J.-L. Casanova, X-linked susceptibility to mycobacteria is caused by mutations in NEMO impairing CD40-dependent IL-12 production. *J. Exp. Med.* **203**, 1745–1759 (2006).
82. M. Imamura, T. Kawai, S. Okada, K. Izawa, T. Takachi, H. Iwabuchi, S. Yoshida, R. Hosokai, H. Kanegane, T. Yamamoto, H. Umezu, R. Nishikomori, T. Heike, M. Uchiyama, C. Imai, Disseminated BCG infection mimicking metastatic nasopharyngeal carcinoma in an immunodeficient child with a novel hypomorphic NEMO mutation. *J. Clin. Immunol.* **31**, 802–810 (2011).
83. J. Bustamante, S. Boisson-Dupuis, L. Abel, J.-L. Casanova, Mendelian susceptibility to mycobacterial disease: Genetic, immunological, and clinical features of inborn errors of IFN-γ immunity. *Semin. Immunol.* **26**, 454–470 (2014).
84. J. Noad, A. von der Malsburg, C. Pathe, M. A. Michel, D. Komander, F. Randow, LUBAC-synthesized linear ubiquitin chains restrict cytosol-invading bacteria by activating autophagy and NF-κB. *Nat. Microbiol.* **2**, 17063 (2017).
85. S. J. L. van Wijk, F. Fricke, L. Herhaus, J. Gupta, K. Hotte, F. Pampaloni, P. Grumati, M. Kaulich, Y.-s. Sou, M. Komatsu, F. R. Greten, S. Fulda, M. Heilemann, I. Dikic, Linear ubiquitination of cytosolic *Salmonella* Typhimurium activates NF-κB and restricts bacterial proliferation. *Nat. Microbiol.* **2**, 17066 (2017).
86. O. Pampliega, I. Orhon, B. Patel, S. Sridhar, A. Díaz-Carretero, I. Beau, P. Codogno, B. H. Satir, P. Satir, A. M. Cuervo, Functional interaction between autophagy and ciliogenesis. *Nature* **502**, 194–200 (2013).
87. O. Pampliega, A. M. Cuervo, Autophagy and primary cilia: Dual interplay. *Curr. Opin. Cell Biol.* **39**, 1–7 (2016).
88. K. F. Winklhofer, I. H. Henn, P. C. Kay-Jackson, U. Heller, J. Tatzelt, Inactivation of parkin by oxidative stress and C-terminal truncations: A protective role of molecular chaperones. *J. Biol. Chem.* **278**, 47199–47208 (2003).

Acknowledgments: We thank I. Dikic for SHARPIN KO (cpdm) MEFs and K. Schork and M. Eisenacher (supported by de.NBI, grant number FKZ 031 A 534A) for help with statistics. **Funding:** The research leading to these results has received funding from the German Research Foundation (WI-2111/4 and WI-2111/6 to K.F.W., MA-3257/5 to K.M., TA-167/6 to J.T., and SFB 1177, project C2 to L.S.), the Michael J. Fox Foundation (Parkin Biology 2013 Grant and Grant ID 16293 to K.F.W.), the Munich Cluster for Systems Neurology (to K.F.W.), the LOEWE program Ub-Net (to L.S.), and PURE (Protein Unit for Research in Europe), a project of North Rhine-Westphalia, Germany (to K.M. and K.B.). Gefördert durch die Deutsche Forschungsgemeinschaft (DFG) im Rahmen der Exzellenzstrategie des Bundes und der Länder–EXC 2033–Projektnummer 390677874–RESOLV. **Author contributions:** K.F.W. and J.T. conceived and supervised the project. J.M., M.S., N.F., T.M., D.A.S., V.B., L.A.B., A.K.M.-R., A.P., A.S., K.B., K.M., and L.S. designed the experiments, performed the research, and analyzed the data. K.R. and F.I. contributed to the data analysis and interpretation. B.K. expressed and purified the recombinant UBAN domain. K.F.W. wrote the manuscript. All authors contributed to the experimental design, data analysis, and interpretation of the results. **Competing interests:** The authors declare that they have no competing interests. **Data and materials availability:** All data needed to evaluate the conclusions in the paper are present in the paper or the Supplementary Materials. The anti–M1-ubiquitin monoclonal 1F11/3F5/Y102L antibody requires a material transfer agreement from Genentech, USA (MTA no. OR-215185).

Submitted 16 August 2018
Accepted 8 January 2020
Published 4 February 2020
10.1126/scisignal.aav1256

Citation: J. Meschede, M. Šadić, N. Furthmann, T. Miedema, D. A. Sehr, A. K. Müller-Rischart, V. Bader, L. A. Berlemann, A. Pilsl, A. Schlierf, K. Barkovits, B. Kachholz, K. Rittinger, F. Ikeda, K. Marcus, L. Schaefer, J. Tatzelt, K. F. Winklhofer, The *parkin-coregulated gene* product PACRG promotes TNF signaling by stabilizing LUBAC. *Sci. Signal.* **13**, eaav1256 (2020).

Science Signaling

The *parkin-coregulated gene* product PACRG promotes TNF signaling by stabilizing LUBAC

Jens Meschede, Maria Sadic, Nikolas Furthmann, Tim Miedema, Dominik A. Sehr, A. Kathrin Müller-Rischart, Verian Bader, Lena A. Berlemann, Anna Pilsl, Anita Schlierf, Katalin Barkovits, Barbara Kachholz, Katrin Rittinger, Fumiyo Ikeda, Katrin Marcus, Liliana Schaefer, Jörg Tatzelt and Konstanze F. Winklhofer

Sci. Signal. **13** (617), eaav1256.
DOI: 10.1126/scisignal.aav1256

Stabilizing LUBAC

The *parkin-coregulated gene* (*PACRG*) encodes a protein of unknown function and shares a promoter with *parkin*, which encodes an E3 ubiquitin ligase that induces the degradation of damaged mitochondria and promotes nuclear factor κB (NF-κB) signaling. Meschede *et al.* found that PACRG played no role in mitophagy in cultured human cells but did promote NF- κB signaling downstream of the tumor necrosis factor (TNF) receptor TNFR1. PACRG was recruited to the TNFR1 signaling complex and protected cells from TNF-induced apoptosis by interacting with and stabilizing the linear ubiquitin chain assembly complex (LUBAC). PACRG functionally substituted for the LUBAC component and adaptor protein SHARPIN. That Parkin and PACRG both promote NF- κB signaling is consistent with previous reports linking polymorphisms in the regulatory regions of both genes with increased susceptibility to infections with intracellular bacterial pathogens.